

 Open access • Journal Article • DOI:10.1039/C1JM11845E

## Magnetic nanoparticles: recent advances in synthesis, self-assembly and applications

— [Source link](#) 

Srikanth Singamaneni, Valery N. Bliznyuk, Christian Binek, Evgeny Y. Tsymbal





**Institutions:** Washington University in St. Louis, Western Michigan University, University of Nebraska–Lincoln

**Published on:** 18 Oct 2011 - Journal of Materials Chemistry (The Royal Society of Chemistry)

**Topics:** Magnetic nanoparticles and Magnetic force microscope

Related papers:

- [Magnetic nanoparticles: Synthesis, protection, functionalization, and application](#)
- [Magnetic nanoparticles: synthesis, functionalization, and applications in bioimaging and magnetic energy storage](#)
- [Magnetic Iron Oxide Nanoparticles: Synthesis, Stabilization, Vectorization, Physicochemical Characterizations, and Biological Applications](#)
- [Biological applications of magnetic nanoparticles](#)
- [Ultra-large-scale syntheses of monodisperse nanocrystals.](#)

Share this paper:    

View more about this paper here: <https://typeset.io/papers/magnetic-nanoparticles-recent-advances-in-synthesis-self-46j74hddet>

6-20-2011

# Magnetic nanoparticles: recent advances in synthesis, self-assembly and applications

Srikanth Singamaneni

*Washington University in St. Louis, singamaneni@wustl.edu*

V. Bliznyuk

*Western Michigan University, Kalamazoo, MI*

Christian Binek

*University of Nebraska-Lincoln, cbinek@unl.edu*

Evgeny Y. Tsymbal

*University of Nebraska-Lincoln, tsymbal@unl.edu*

Follow this and additional works at: <http://digitalcommons.unl.edu/physicsbinek>

---

Singamaneni, Srikanth; Bliznyuk, V.; Binek, Christian; and Tsymbal, Evgeny Y., "Magnetic nanoparticles: recent advances in synthesis, self-assembly and applications" (2011). *Christian Binek Publications*. 84.

<http://digitalcommons.unl.edu/physicsbinek/84>

This Article is brought to you for free and open access by the Research Papers in Physics and Astronomy at DigitalCommons@University of Nebraska - Lincoln. It has been accepted for inclusion in Christian Binek Publications by an authorized administrator of DigitalCommons@University of Nebraska - Lincoln.

Cite this: *J. Mater. Chem.*, 2011, **21**, 16819

www.rsc.org/materials

## Magnetic nanoparticles: recent advances in synthesis, self-assembly and applications

Srikanth Singamaneni,<sup>\*a</sup> Valery N. Bliznyuk,<sup>\*b</sup> Christian Binck<sup>c</sup> and Evgeny Y. Tsymbal<sup>c</sup>

Received 27th April 2011, Accepted 20th June 2011

DOI: 10.1039/c1jm11845e

Nanostructured magnetic materials have a variety of promising applications spreading from nano-scale electronic devices, sensors and high-density data storage media to controlled drug delivery and cancer diagnostics/treatment systems. Magnetic nanoparticles offer the most natural and elegant way for fabrication of such (multi-) functional materials. In this review, we briefly summarize the recent progress in the synthesis of magnetic nanoparticles (which now can be done with precise control over the size and surface chemistry), and nanoscale interactions leading to their self-assembly into 1D, 2D or 3D aggregates. Various approaches to self-organization, directed-, or template-assisted assembly of these nanostructures are discussed with the special emphasis on magnetic-field enabled interactions. We also discuss new physical phenomena associated with magnetic coupling between nanoparticles and their interaction with a substrate and the characterization of the physical properties at the nanoscale using various experimental techniques (including scanning quantum interferometry (SQUID) and magnetic force microscopy). Applications of magnetic nanoparticle assemblies in data storage, spintronics, drug delivery, cancer therapy, and prospective applications such as adaptive materials and multifunctional reconfigurable materials are also highlighted.

<sup>a</sup>Department of Mechanical Engineering and Materials Science, Washington University in St Louis, MO, USA. E-mail: singamaneni@wustl.edu

<sup>b</sup>Department of Materials Science and Engineering, Western Michigan University, Kalamazoo, MI, USA. E-mail: valery.bliznyuk@wmich.edu

<sup>c</sup>Department of Physics and Astronomy, Nebraska Center for Materials and Nanoscience, University of Nebraska, Lincoln, NE, USA

### 1. Introduction

The interest in nanostructured materials is driven by unusual physical properties of highly confined systems with reduced dimensionality as well as by their promising applications in electronics, optics, energy conversion and storage. Nanoparticles



Srikanth Singamaneni

Srikanth Singamaneni received his PhD in Polymer Materials Science and Engineering at Georgia Institute of Technology in 2009, and he is currently an assistant professor in the Department of Mechanical Engineering and Materials Science, Washington University in St Louis. He has co-authored nearly 60 refereed articles in archival journals. He is a recipient of the Materials Research Society (MRS) graduate student gold award, Fall 2008, and MRS Best-Poster Award at

the National Meeting, Spring 2007. His current scientific interests include chemical and biological sensors based on nanomaterials and confinement effects in polymers and polymer nanocomposites.



Valery N. Bliznyuk

Valery Bliznyuk is an associate professor at Western Michigan University, Kalamazoo, Michigan since 2001; received PhD degree in Polymer Science from the Institute of Macromolecular Chemistry of National Academy of Sciences, Kiev, Ukraine (1985), and DSc degree in Polymer Chemistry in the field of nanostructured organic materials from Kiev State University (2004); worked as a researcher in Ukraine, Germany (Alexander von Humboldt Foundation fellow, University of

Mainz), England (University of Cambridge, and University of Oxford), and the USA. He is a co-author of more than 100 peer-reviewed publications and several reviews in the field of nanostructured materials and their characterization.

can be used directly or also as building blocks to construct nanostructured materials (arrays of nanoparticles) with unique properties suitable for many modern applications spreading from photonic crystals<sup>1</sup> to cosmetics and biomedical research (especially gold colloids).<sup>2</sup> Self-assembly (also known as a “bottom up” fabrication process) is technologically the most attractive way for construction of such nanostructured materials as it provides scalability and simplicity for the fabrication of complex (hierarchical) structures.<sup>3–5</sup> Magnetic nanoparticles, which are considered in this review, are no exception and offer interesting current and future applications in high-density data storage, nanoscale electronics, sensors, and medicine.<sup>6–11</sup>

Magnetic properties of nanoparticles depend strongly on their size and shape in addition to their intrinsic magnetic characteristics, such as magnetic moment and magneto-crystalline anisotropy. Magnetic moments of individual atoms constituting a nanoparticle can be coupled *via* the exchange interaction so that the particle as the whole may possess a super-atomic scale magnetic moment (a “superspin”). The magnetic anisotropy energy associated with such a superspin can have a small value comparable to the thermal energy. It depends on the number of coupled atomic spins and therefore on the size of the nanoparticle as well as the anisotropy constant. When temperature is decreased in the presence of a magnetic field, such a nanomagnetic ensemble may become magnetically ordered below some limiting temperature known as the blocking temperature,  $T_b$ , and can maintain remanent magnetization even if the field is removed. Sufficiently small nanoparticles have a single domain structure as opposed to larger particles, which can be divided into several domains with different magnetization orientations

(Fig. 1). Single-domain particles are characterized with a preferred axis of magnetization (the so-called ‘easy’ axis), which depends on the nature of the material and the shape of the particle. Several typical shapes and magnetization orientations are shown in Fig. 1. The preferred orientation of magnetization in elongated particles (nanorods) with a large aspect ratio (the ratio of their height to diameter) is parallel to the long axis of such a nanorod if the shape anisotropy dominates over the crystalline anisotropy. For disc-like particles with a small aspect ratio the shape anisotropy favors in-plane magnetization.<sup>12</sup> The magnetic energy of the nanoparticle varies depending on the angle  $\theta$  of deviation of the magnetization direction from the easy axis and an effective anisotropy constant  $K$  as  $E(\theta) = KV \sin^2(\theta)$ , where  $V$  is the volume of the particle. Therefore, for an easy axis particle one can imagine two preferred orientations for the superspin: “up” and “down” (or  $\theta = 0$  and  $\theta = \pi$ ) separated by the energy barrier  $KV$ . At high temperature, thermal fluctuations cause fast flipping of the magnetization between these two energy minima, but at lower temperature, the superspin is “frozen” (blocked) in one of the minima.

A characteristic time  $\tau$  for the superspin flipping obeys the Arrhenius law:  $\tau = \tau_0 \exp(E_B/kT)$ , where  $E_B$  is the height of the energy barrier ( $E_B = KV$  if no external magnetic field is applied), and  $\tau_0$  is a material-specific relaxation time, which is of the order of  $10^{-9}$  s for a 10 nm size particles.<sup>13</sup> The characteristic time scale should be compared to the relevant experimental time scale  $\tau_{\text{exp}}$ . When  $\tau$  is larger than  $\tau_{\text{exp}}$  the magnetic moment of the particle is blocked exhibiting apparent ferromagnetic behavior with characteristic hysteresis in the magnetization curve upon changes in the applied magnetic field. In contrast, when the experimental



**Christian Binek**

*Christian Binek received his PhD in physics in 1995 followed six years later by his certificate of Habilitation at the University of Duisburg, Germany. Dr Binek is currently an associate professor in the Department of Physics and Astronomy at the University of Nebraska—Lincoln. His major contributions are in the field of magnetic heterostructures, spintronics and fundamental aspects of thermodynamics and statistical mechanics. This is documented in more than 75 publications in*

*peer reviewed journals, book chapters, and a monograph entitled “Ising-type Antiferromagnets: Model Systems in Statistical Physics and in the Magnetism of Exchange Bias” published in 2003 in the Springer Series STMP. Dr Binek received in 1996 the annual award of the society of the University Duisburg for his outstanding PhD thesis, the NSF career award in 2006, and the 2007 Sigma Xi Outstanding Junior Investigator Award. Dr Binek is leader of the interdisciplinary research group two of the NSF funded materials research science and engineering center (MRSEC) at the University of Nebraska.*



**Evgeny Y. Tsymbal**

*Evgeny Tsymbal is Charles Bessey Professor at the Department of Physics and Astronomy of the University of Nebraska—Lincoln (UNL) and Director of the UNL’s Materials Research Science and Engineering Center (MRSEC). His research is focused on computational materials science aiming at the understanding of fundamental properties of advanced ferroic heterostructures relevant to nano-electronics and spintronics. He has published over 150 papers*

*and presented over 100 invited talks on these subjects. His research has been supported by the National Science Foundation, Semiconductor Research Corporation, the Office of Naval Research, the Department of Energy, Seagate Technology, and the W. M. Keck Foundation. Evgeny Tsymbal is a fellow of the American Physical Society, a fellow of the Institute of Physics, UK, and a recipient of the UNL’s College of Arts & Sciences Outstanding Research and Creativity Award (ORCA).*

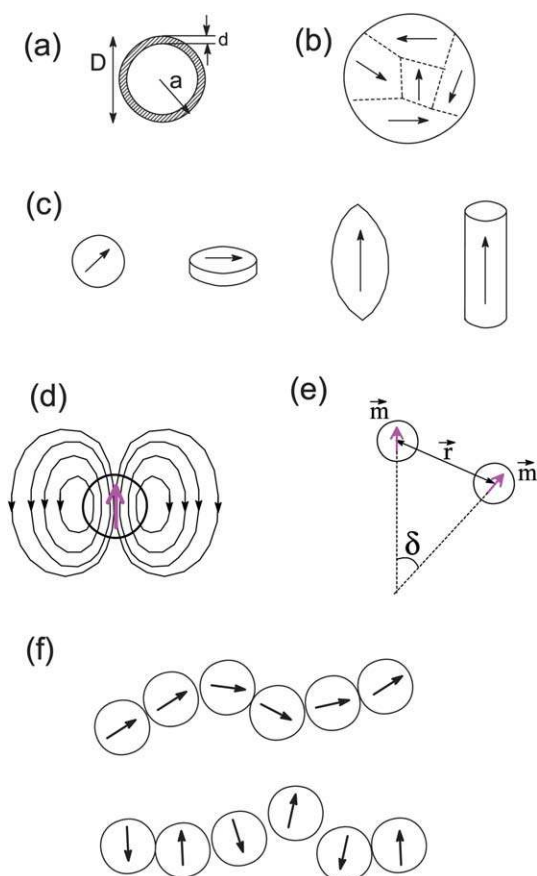


**Fig. 1** (a) Individual single-domain magnetic nanoparticle coated with a non-magnetic (metal oxide or organic ligand) shell of thickness  $d$ ; (b) scheme of polydomain ferromagnetic nanoparticle; (c) different common shapes of magnetic nanoparticles (from left to right: spherical or polygonal, disk-like, ellipsoidal and nanorod). Arrows inside show the easy-axis magnetization direction; (d) distribution of the magnetic field lines around a single domain magnetic nanoparticle; (e) schematic of magnetic interaction between two single-domain magnetic nanoparticles; (f) two of the most common scenarios for magnetic self-assembly with a head-to-tail arrangement of magnetic dipole moments (top) and antiparallel arrangement of magnetic dipole moments (bottom).

time scales are much larger than the relaxation time, the super-spin fluctuates frequently on the experimental time scale such that the time-average magnetic moment,  $\mathbf{m}$ , is equal to zero. This consideration defines two distinguished magnetic behaviors: a superparamagnetically blocked state below  $T_b$  and superparamagnetic state above this temperature. The superparamagnetic transition depends therefore on the nature of the material, the size and the shape of the nanoparticles and can be described in terms of the smallest size of the nanoparticles (when they are still blocked at room temperature) or in terms of the temperature at which the superparamagnetic transition occurs for a given average size of the particles.

Fig. 2 shows how the critical size for superparamagnetic transition ( $D_{sp}$ ) depends on the type of the material for several common ferromagnetic materials. It demonstrates also another transition between a single-domain and polydomain state,  $D_{cryt}$ .<sup>9</sup> As follows from this consideration, nanoparticles of 10–15 nm in diameter with effective anisotropies typical for 3d ferromagnets

have the blocking temperature<sup>14</sup> much below the room temperature.<sup>15</sup> For such a case the individual particle dipoles are randomly oriented due to thermal fluctuations and hence, a collection of such nanoparticles does not possess a net magnetic moment unless an external magnetic field aligning the individual dipole moments of the nanoparticles is applied.

According to this consideration, the blocking temperature  $T_b$  can be defined as:  $T_b = KV/k_B \ln(\tau_{exp}/\tau_0)$ , where  $k_B$  is the Boltzmann constant. For example,  $T_b$  of 26 nm  $Fe_3O_4$  nanoparticles ( $K \approx 1.1 \times 10^4 \text{ J m}^{-1}$ )<sup>16</sup> is about 300 K and, therefore, particles larger than  $\sim 26$  nm are predicted to have ferromagnetic behavior at room temperature, while smaller particles should exhibit superparamagnetism.<sup>27</sup> Similar to paramagnetic atoms and molecules, arrays of nanoparticles in superparamagnetic state exhibit a net magnetic moment only under an applied magnetic field. The magnetization vector  $\mathbf{M}$  (the magnetic moment per unit volume) of an array of non-interacting nanoparticles in the absence of magnetic anisotropy obeys the Langevin equation.<sup>10,17</sup>

$$M = M_{sat} \varphi (\cot h(\alpha) - 1/\alpha) \quad (1)$$

where  $\varphi$  is the volume fraction of magnetic particles,  $M_{sat}$  is the bulk saturation magnetization of the particle material and the Langevin parameter,  $\alpha$ , depends on the radius of a nanoparticle,  $a$ , temperature and external magnetic field strength,  $H$ :

$$\alpha = \frac{4\pi a^3}{3} \frac{\mu_0 M_{sat} |H|}{k_B T} \quad (2)$$

when the nanoparticles are put into external magnetic field  $H$ , they acquire induced magnetic moments  $m = \mu_0 \chi V H = \mu_0 M_{sat} V$  (where  $\mu_0$  is magnetic permeability of vacuum,  $\chi$  is the material susceptibility, and  $V$  is the particle volume). Therefore, the magnitude of the intrinsic magnetic moment scales with the particle volume.

Magnetized particles themselves can act as small magnets. The energy of interaction between two magnetized particles is described with a Keesom potential, which depends on the strength of dipole moments, and scales as  $r^{-3}$  with the distance between them (Fig. 1e). The interaction between magnetized

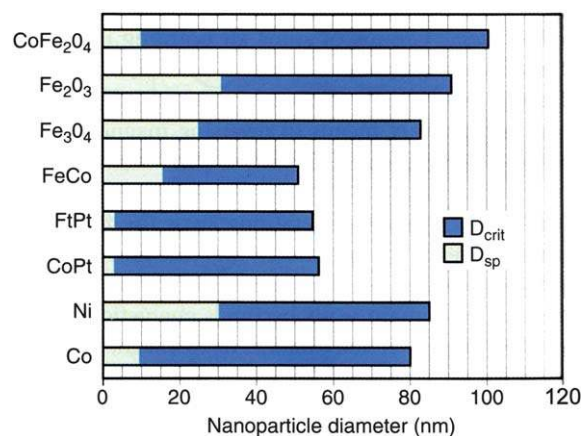


**Fig. 2** Single domain size  $D_{crit}$  and superparamagnetic limit at room temperature,  $D_{sp}$  for common ferromagnetic materials. Reprinted from ref. 9.



nanoparticles depends strongly on their relative orientation (may be attractive or repulsive depending on the angle  $\delta$ ). The force of the dipole–dipole interaction  $F = -\nabla U_{\text{mag}}$  scales as  $r^{-4}$ , indicating that it becomes much stronger as two nanoparticles are close to each other. The strength of the inter-particle interaction can be also characterized by the dimensionless dipole strength parameter:  $\lambda = (\pi\mu_0 a^3 \chi^2 H^2) / 9k_B T$ .<sup>18</sup>

Within the material, spins can be strongly coupled and therefore orient collectively in a single direction (the easy magnetization direction<sup>†</sup>). Contrary to this behavior, spins are increasingly disordered near the nanoparticle surface due to weaker coupling with the more ordered interior spins. As a result of such a surface effect, the saturation magnetization of a nanoparticle  $M_{\text{sat}}$  is smaller than the corresponding bulk value  $M_{\text{sat}}^{\text{bulk}}$  and can be approximated as:  $M_{\text{sat}} = M_{\text{sat}}^{\text{bulk}} [(a - d)/a]^3$ , where  $a$  is the radius of the particle, and  $d$  is a characteristic thickness of the disordered surface layer (see Fig. 1a).<sup>19</sup> The thickness of the disordered layer may be different depending on the type of the particles but is typically on the order of 1–2 nm.<sup>20,21</sup>

The nanoparticles are often coated with adsorbed surfactant layers or have a natural oxide layer on the surface. The surfactant (or ligand) layer is often intentionally produced during nanoparticles synthesis in order to prevent their agglomeration that would otherwise occur due to the attractive van der Waals forces and dipole–dipole interactions. In many cases the nanoparticles are additionally “functionalized”, *i.e.*, coated with suitable inorganic or organic molecules that serve specific chemical or biological tasks.<sup>22</sup>

If ferromagnetic nanoparticles are suspended in a liquid (so-called ferrofluids) they may possess additional degrees of freedom associated with possible rotation of the nanoparticles and therefore the effective blocking temperature may be smaller. In this case even strongly coupled nanoparticles of relatively big size may display superparamagnetic behavior due to possible relaxation *via* rotational diffusion of the entire particle (instead of its moment). In this case the characteristic relaxation time depends on the viscosity  $\eta$  of the imbedding fluid:  $\tau = 3V\eta/k_B T$ .<sup>27</sup> On the other hand, if the same nanoparticles are densely packed or are adsorbed on a surface of some solid (template) the  $T_b$  may be enhanced. For example, closely packed arrays of magnetite nanoparticles exhibit ferromagnetic behavior even for particles smaller than  $D_{\text{sp}} = 26$  nm due to strong dipole–dipole interactions.<sup>23</sup> Skumryev *et al.* demonstrated that confined magnetic Co nanoparticles embedded in an antiferromagnetic matrix (CoO) can lead to a significant, up to 30-fold, increase of the blocking temperature in comparison to a paramagnetic ( $\text{Al}_2\text{O}_3$ ) matrix environment.<sup>24</sup> The effect is due to a strong exchange interaction in the system causing pinning of the nanoparticles magnetic moments by the matrix. As mentioned by Eisenmenger and Schuller, similar effects should be observed for 2D and 3D arrays of monodisperse nanoparticles where coupling between the nanomagnets cannot be completely ignored.<sup>25</sup> As an additional factor, immobilization of nanoparticles on a solid substrate also implies reducing the number of their degrees of freedom (*e.g.*, due to eliminating rotational degrees of freedom in comparison to a ferrofluid case) and therefore leads to increase of  $T_b$ .<sup>26</sup>

<sup>†</sup> Much more complicated spin structures have been found (*e.g.*, “flower state”) even in so-called single domain particles.

Being a nanoscale magnet, individual nanoparticle generates a local magnetic field, which can be represented with magnetic field lines (Fig. 3). Calculations show that this magnetic field produces attractive interaction to other similar nanomagnets if they are located near the poles along the main magnetization axis. Simultaneously a repulsive interaction will be observed with other nanoparticles located near the equator as shown in Fig. 3.<sup>27</sup>

## 2. Synthesis of magnetic nanostructures

Numerous approaches such as chemical, template-assisted and lithographic have been extensively investigated for the fabrication of a wide variety of magnetic nanostructures such as iron oxide, pure metal, metal alloys and core–shell structures. Although a comprehensive literature review of the various synthetic routines is beyond the scope of this review, we will briefly describe the most important methods, which have offered excellent size and shape control.

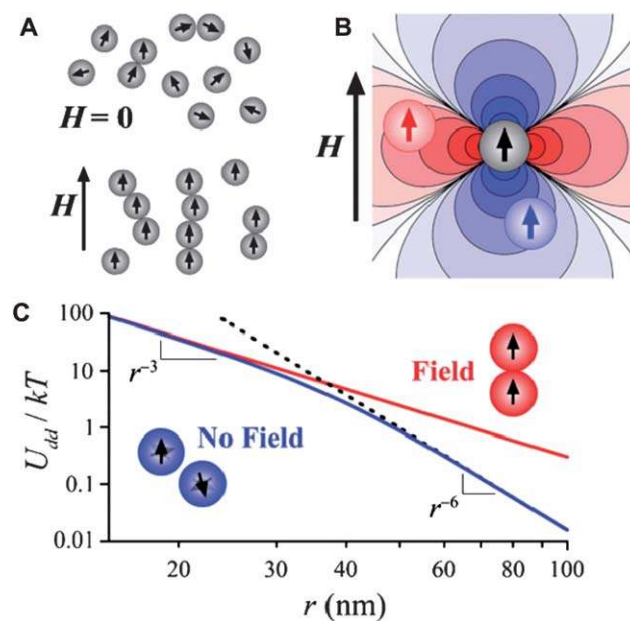


**Fig. 3** (A) Cooperative behavior of weakly interacting magnetic nanoparticles in a liquid dispersion under or without external magnetic field (if the magnetic field is zero nanoparticles are randomly oriented, while in the presence of the magnetic field they prone to form chains); (B) computer simulation of an interaction potential distribution around a single domain magnetic nanoparticle. Blue regions near the poles of the particle correspond to attraction interaction while red regions near the equator correspond to repulsion. (C) Interaction potential acting between two 15 nm cobalt nanoparticles with a magnetization of  $1.4 \times 10^6 \text{ Am}^{-1}$  depending on the distance between them. At small separations interaction is strong (and scales as  $r^{-3}$ ) causing in-line alignment of neighboring particles. At larger separations the magnetic moments become increasingly disordered and their interaction is better described with nonmagnetic van der Waals interactions (dashed curve), which scales as  $r^{-6}$  with the inter-particle distance. However, the transition from  $r^{-3}$  to  $r^{-6}$  regime is not observed in the presence of an external magnetic field, which maintains coupling and relative orientation of the magnetic dipoles at any separation. Reprinted from ref. 27.

## 2.1 Chemical synthesis

Chemical synthesis of nanostructures has been achieved using techniques such as thermal decomposition, co-precipitation, microemulsion and hydrothermal methods.<sup>28</sup> Thermal decomposition and hydrothermal approaches offer better shape and size (narrow distribution of the size of the particles) compared to other synthetic routes. Narrow distribution of the size of magnetic nanoparticles is important considering the fact that the blocking temperature of nanomagnets critically depends on the size of the particles and a polydisperse sample results in broad blocking temperature, a trait undesirable in most of the applications.

Thermal decomposition method involves in the synthesis of monodisperse magnetic nanostructures by thermal decomposition of organometallic compounds such as acetylacetonates, carbonyls or cuproferonates in organic solvents in the presence of surfactants such as oleic acid and hexadecylamine.<sup>29–32</sup> The ratio of various precursors involved in the reaction governs the size and shape of nanostructures formed in the process. A general decomposition approach for the synthesis of size- and shape controlled magnetic oxide nanocrystals has been reported by Peng and co-workers.<sup>33</sup> The technique is based on the pyrolysis of metal fatty acid salts in the presence of corresponding fatty acids (lauric acid, myristic acid, decanoic acid, palmitic acid, oleic acid, stearic acid), a hydrocarbon solvent (*e.g.* octadecene), and activation reagents. Nanocrystals with very narrow size distribution and sizes tunable over a wide size range (3–50 nm) could be synthesized. Furthermore the technique offered excellent control over the shape (spherical particles, cubes) of the nanocrystals.

In a more recent study, Nogués and co-workers have synthesized highly monodisperse (both in terms of shape and size) cubic and spherical maghemite ( $\gamma\text{-Fe}_2\text{O}_3$ ) nanocrystals using thermal decomposition method.<sup>34</sup> The ratio of the precursors (iron oleate and oleic acid) and the thermal decomposition time were varied to achieve shape controlled nanocrystals. In particular, decomposition for shorter duration (2 hours) resulted in spherical particles while decomposition for longer duration (10 hours) resulted in cubic particles. Fig. 4 shows the high resolution TEM images of the spherical and cubic maghemite nanocrystals obtained using the thermal decomposition method. The saturation magnetization, coercivity, and hysteresis loop shift remained largely insensitive to the shape of the nanocrystals. However, the blocking temperature of the spherical particles was found to be significantly higher compared to the nanocubes despite having similar volume. Control of the surface anisotropy of nanocrystals also offers unique opportunities in the self-assembly of nanocrystals, often not accessible to spherical particles.<sup>35</sup>

Apart from metal oxide magnetic nanocrystals, thermal decomposition technique was also employed for the synthesis of shape controlled metal nanocrystals. Magnetic nanoparticles of 3d transition metals (Co, Ni, Fe) were synthesized by introducing a reducing agent into a hot solution of metal precursor and surfactant, which results in a single short nucleation event followed by slow growth process. Excellent control over the size and shape of the nanoparticles has been achieved by precisely choosing the temperature and metal precursor to surfactant ratio.<sup>36–39</sup> One note worthy example, which subsequently led to

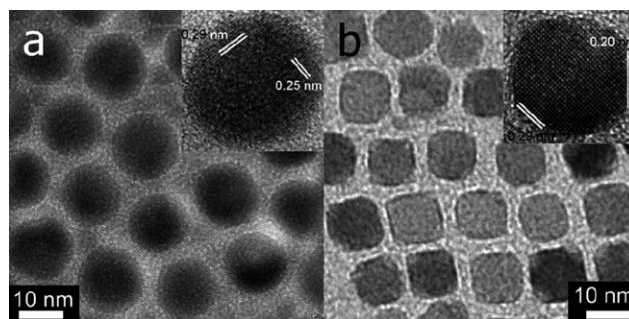


**Fig. 4** High resolution TEM images showing the monodisperse (a) nanospheres and (b) nanocubes obtained by thermal decomposition method. Reprinted from ref. 34.

significant developments, is the cobalt nanoplates synthesized by Alivisatos and co-workers using thermal decomposition of cobalt carbonyl precursor.<sup>37</sup> From their initial study, the authors noted three important factors for achieving shape controlled magnetic nanocrystals: (i) presence of suitable organometallic precursor that decomposes at temperatures below the surfactants' degradation temperature; (ii) two surfactants that differentially adsorb to the nanocrystal faces; and (iii) one of the surfactants must promote monomer exchange between particles to allow narrow size distribution. In subsequent studies, highly monodisperse cobalt and nickel nanorods have been synthesized using thermal decomposition approach by various groups.<sup>40–42</sup> Such chemically synthesized nanostructures show minute magnetic interaction due to dilution and separation of nanoparticles in the solvent.

The other important chemical synthesis approach, which offers excellent control over the size and shape of the nanocrystals is the hydrothermal synthesis, which involves the use of liquid–solid–solution (LSS) reaction. This truly versatile approach for the synthesis of a wide variety of nanocrystals such as metallic, semi-conducting, dielectric, magnetic, rare-earth fluorescent and polymeric was introduced by Li and co-workers.<sup>43</sup> The general strategy involves LSS reaction at different reaction and temperature conditions. In particular, the preparation of metal nanocrystals involved the reduction of metal ions by ethanol at the interfaces of metal linoleate (solid), ethanol–linoleic acid liquid phase (liquid) and water–ethanol solutions (solution) at different temperatures under hydrothermal conditions. The strategy is based on the phase separation occurring at the interface of solid–liquid–solution phases present in the reaction. As an example, the authors have demonstrated the synthesis of monodisperse ( $\sim 10$  nm)  $\text{Fe}_3\text{O}_4$  and  $\text{CoFe}_2\text{O}_4$  nanocrystals.

Singamaneni and Bliznyuk have demonstrated an unconventional and facile approach to synthesize magnetic nanocrystals with uniform size.<sup>44</sup> Ni nanoparticles with 10 nm diameter were synthesized by ultrasonication of the thermally evaporated Ni film in an organic solvent (chloroform). The authors suggested that initially when the glass substrate with Ni film is placed in the solvent, liquid bridges the gaps between the grains due to capillary forces. Ultrasonic agitation causes the liquid filling the interstices to exert pressure on the adjacent grains and subsequently move the particle. The ultrasonic energy overcomes the

weak van der Waals interaction between Ni grains on the glass substrate, causing the Ni grains to be removed from the substrate and colloidally suspending them in the solvent. The nanoparticles suspended in the solution have been assembled into nanochains using an external magnetic field as will be discussed in Section 3.

## 2.2 Template assisted fabrication

The other important approach is the template-assisted fabrication of nanostructures.<sup>45</sup> The technique offers two important advantages compared to the chemical routes: (i) the size and shape of the nanostructures formed are predetermined by the template chosen for the purpose and (ii) complex nanostructures such as nanobarcodes (segmented nanowires with precise control of the composition along the length) can be fabricated with relative ease. On the other hand, template assisted methods suffer from the inherent drawback of being inherently a two-step process that involves the fabrication of high quality templates and subsequent deposition of magnetic material within the template. While several templates such as anodic aluminium oxide (AAO) and highly oriented pyrolytic graphite (HOPG) are commercially available, the choices (diameter of the pores, thickness, uniformity) are rather limited forcing in-house fabrication of the templates. The readers are referred to elsewhere for a comprehensive discussion of various template assisted nanofabrication methods.<sup>46–48</sup> In the following discussion, we highlight few important recent developments in the template-assisted fabrication of complex magnetic nanostructures.

There have been numerous demonstrations of magnetic nanowires deposited using anodic alumina oxide as the so-called hard template.<sup>49–51</sup> Mirkin and co-workers have fabricated nanobarcodes (segmented nanorods) comprised of various magnetic and non-magnetic (metals and polymers) components.<sup>52</sup> In a recent study, Bangar *et al.* have fabricated multi-component nanowires comprised of gold, nickel and polypyrrole.<sup>53</sup> Fig. 5 shows the general strategy for the fabrication of such multi-segmented nanorods, which involves the deposition of a thin seed gold layer (sputtered or thermally evaporated) on one of the surfaces of the anodic alumina template. Subsequently, the material of interest is electrodeposited into the pores. In the case of segmented nanowires (barcodes), the electrodeposition (electrochemical polymerization) of the material is ceased at a precise length followed by the deposition of the subsequent metal or polymer. Finally, the gold seed layer is mechanically removed and the nanobarcodes are freed from the template by dissolving the template using basic solution (typically aqueous NaOH or KOH). The so formed nanowires can be functionalized and reassembled for various applications.

Highly oriented pyrolytic graphite (HOPG) was introduced by Penner and co-workers as a different class of template for the fabrication of highly oriented metal (Au, Ag, Cu, Pd, Ni) and metal oxide (MoO<sub>2</sub>) nanowires.<sup>54,55</sup> The technique involves the electrodeposition of metal nanoparticles, which eventually fuse to form metal nanowires, at the step edges of HOPG.<sup>56–58</sup> The preferential nucleation of the nanoparticles at the step edges is favored owing to the extremely low surface energy of the basal plane of graphite and relatively high activity of the step edges (which act as nucleation defects and also catalyze the electron

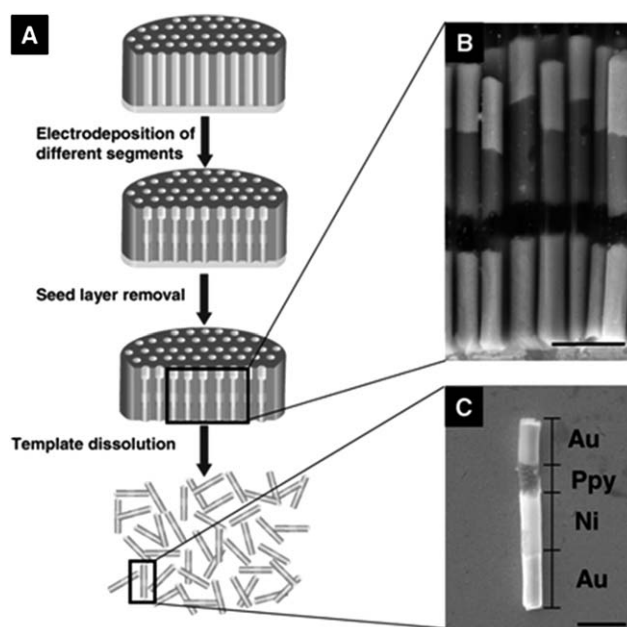


**Fig. 5** (A) Schematic of different steps involved in synthesis and suspension of multisegmented nanowires. (B) Cross-sectional SEM image of four segment nanowires inside the alumina template. (C) SEM image of single suspended nanowire showing different segments of the nanowire. (Scale bar = 1  $\mu\text{m}$ .) Reprinted from ref. 52.

transfer to metal ions from solution). Fig. 6 shows the general strategy involved in the fabrication of metal nanowires using HOPG template and SEM image of Ni nanowires fabricated using this approach. Nickel nanowires of different diameters were synthesized by this technique by controlling the deposition time.<sup>59</sup>

Bioengineering approaches involving biomolecules as templates for the fabrication of magnetic nanostructures with well-defined size have been pioneered and extensively investigated by Mann's group. The technique involves in demetallizing iron storage protein, ferritin, followed by remineralization of the desired species in the self-assembled polypeptide shell. The polypeptide shell acts as a template, which determines the size of the nanostructures mineralized within the cage. Numerous materials such as uranium oxide, manganese oxide, and cadmium sulfide have been mineralized forming bio-inorganic

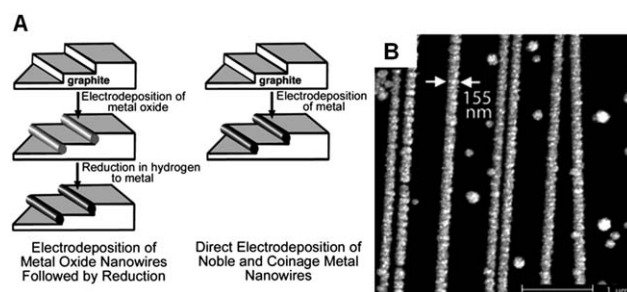


**Fig. 6** (A) Schematic showing the two possible approaches for the fabrication of parallel arrays of metal nanowires on highly oriented pyrolytic graphite (HOPG). (B) SEM image showing the parallel arrays of Ni nanowires deposited on HOPG. Reprinted from ref. 56.



composites.<sup>60–62</sup> Magnetic materials such as maghemite and magnetite have been mineralized within the protein cage to result in so-called magnetoferritins.

In a refined approach, which was subsequently adapted by others, magnetoferritin was synthesized by performing the remineralization process under anaerobic conditions in the presence of stoichiometric amounts of oxidant.<sup>63,64</sup> The process enabled the minimization of the formation of nonmagnetic ferric oxides such as ferrihydrite. Moreover, the reaction involved in a series of cycles of incremental additions of Fe(II) followed by oxidant, which enabled specific nucleation of the magnetic phase within the protein cavity and minimization of precipitation in bulk solution. The resulting material is a dispersion that can be treated as a bioinorganic ferrofluid with significant potential as a biocompatible magnetic resonance contrast agent.

### 3. Assembly of magnetic nanostructures

Self-assembly is a thermodynamically driven process of organization of structural units (building blocks) such as atoms, molecules or nanoparticles into bigger arrays, which may have complex shape and are stabilized against destructive thermal fluctuations *via* nanoscale forces of interaction inherent to the system.<sup>65–69</sup> Self-assembly process can be in many cases stimulated by application of a nanostructured surface (template) or external fields (field-directed or field-assisted assembly).<sup>11,27,70–76</sup> The field (or a combination of several fields) is used in this case to guide the self-organization process and provide a control over the ultimate structures that form, including their dimensionality, anisotropy, and defect density. Self-assembly is at the heart of the so-called “bottom up” nanofabrication approach, which is widely used in the modern nanoscience and nanotechnology.<sup>3</sup>

#### 3.1 Interaction between magnetic nanoparticles and their self-assembly from dispersions

As discussed above, the dominant contribution to interactions between magnetic nanoparticles and the main driving force for self-assembly in nanomagnetic systems originates from magnetostatic dipole–dipole interaction. The dipole–dipole energy of interaction between two nanoparticles with magnetic dipole moments  $m_1$  and  $m_2$  is in this case the work required to bring these two particles from infinity to a finite separation,  $r$ <sup>10</sup>

$$U_{\text{dd}} = \frac{m_1 \cdot m_2 - 3(m_1 \cdot \vec{r})(m_2 \cdot \vec{r})}{4\pi\mu_0 r^3} \quad (3)$$

where  $r$  is the vector connecting particle 1 and 2 and  $\vec{r}$  denotes the unit vector parallel to it. Or, otherwise, for one nanoparticle in external magnetic field  $H$ :  $U_{\text{m}} = -\mu_0 m H$ . The force acting on this nanoparticle is described as a gradient of the energy:  $F = \nabla(mH)$ . The magnetic field can be also created by neighboring nanoparticles. For spherical particles with spatially homogeneous magnetization,  $m$ , and radius  $a$ , this field is given as:<sup>27</sup>

$$H = \frac{3(m \cdot \vec{r})\vec{r} - m}{4\pi\mu_0 r^3} \quad (4)$$

Essential for magnetic dipole–dipole interactions is that they are directional. Also they can be attractive or repulsive depending on the relative orientation of the dipoles in space. As shown in

Fig. 3, parallel (or “in line”) positioning of the dipoles leads to attractive interaction while so-called antiparallel arrangement of the same dipoles produces repulsion between them. The magnitude of the interaction for parallel alignment is twice higher in comparison to the antiparallel one ( $-m^2/2\pi\mu_0 r^3$  versus  $-m^2/4\pi\mu_0 r^3$  in accordance to eqn (3)). The energy of interaction scales linearly with the volume of the particle and therefore may be too weak to induce self-assembly for very small nanoparticles. The estimates show that, for example, for iron oxide particles smaller than  $\sim 7$  nm this energy became smaller than  $kT$ , and therefore, arrangement caused by magnetic interactions will be randomized by their Brownian motion.

As can be seen from eqn (4), for relatively large particles with fixed magnetic moments the dipole–dipole interactions are long-ranged and decay with the distance between them as  $r^{-3}$ . If nanoparticles are in superparamagnetic state, the dipole–dipole interactions are weaker and scale with the distance as  $r^{-6}$  (so-called Keesom interactions):<sup>77</sup>

$$U_{\text{dd}}(r) = -\frac{(m_1 m_2)^2}{48\pi^2 k_B T \mu_0^2 r^6} \quad \text{if} \quad \frac{m_1 m_2}{2\pi\mu_0 r^3} \ll 6k_B T \quad (5)$$

Fig. 3B demonstrates transition from strongly correlated in-line regime of interaction to  $r^{-6}$  dependence for decoherent dipoles when the dipole energy falls below  $\sim 6 kT$  in the case of superparamagnetic particles.<sup>78</sup>

There are two trends in self-assembly process which appear in the case of application of the external magnetic field: first, the external magnetic field may induce formation of nanoparticle arrays even for very small particles which normally (without such field) would not easily aggregate.<sup>79,80</sup> Secondly, oriented anisotropic structures (for example, string phases oriented with respect to the field) are formed. It was even shown that such field-assisted self-assembly process may be reversible. If the characteristic dipole energy of the nanoparticles is within the range of  $\sim 2 kT$  to  $\sim 8 kT$  they can be assembled and disassembled on demand through the application or removal of an applied magnetic field<sup>79</sup> (a similar effect provides the basis for magneto-rheological fluids).<sup>81</sup>

In addition to magnetic interactions, some other interactions have to be included into consideration for magnetic nanoparticles. These may include the van der Waals attraction between metallic cores and the repulsive forces from the surfactant chains. Van der Waals forces become increasingly important with decreasing the particle size. Even a simple consideration of spherical particles coated with a SAM monolayer or any nonmagnetic (defect) layer of the thickness,  $d$ , leads to such conclusion. The surface defect layer prevents the magnetic cores from touching each other; they are at least separated with a distance of  $\sim 2d$ . In accordance to Derjaguin approximation, which is valid when  $d$  is much smaller than the particle diameter,  $a$  ( $d \ll a$ )<sup>27</sup> the magnitude of the van der Waals energy is  $U_{\text{vdw}} \approx -Aa/24d$  (where  $A$  is Hamaker constant of the material in the presence of the surrounding media) and scales linearly with the particle’s radius. On the other hand, the magnetic dipolar interaction energy is proportional to the particle’s volume:  $U_{\text{dd}} \approx -(1/9)\pi\mu_0 a^3 M^2$ . Therefore, van der Waals interactions will dominate for sufficiently small particles and small inter-particle distances, while magnetic interactions are long-range ones and

will play a crucial role on the early stages of self-assembly from liquid dispersions and in the presence of the external magnetic field. For example, as discussed in ref. 79, aggregation of 10 nm  $\gamma$ -Fe<sub>2</sub>O<sub>3</sub> (magnetite) nanoparticles in the absence of the external magnetic field can be attributed mainly to van der Waals interaction between the particles, while the magnetic interactions will dominate and will govern the self-assembly process in this system in the presence of a strong external magnetic field of the order 0.6 T.<sup>79</sup>

Magnetic dipole–dipole interactions are essentially directional in nature. Due to this reason the types of self-assembled nanostructures formed by spherical magnetic colloids are far richer than those which are driven by all-attractive, spherically symmetric potentials of van der Waals interactions. The dipolar attraction is the strongest if the dipoles are put “in-line” configuration, which promotes the nanomagnets to assemble into linear chains<sup>82–85</sup> or ring structures<sup>86,87</sup> from dilute solutions. The type of the morphology depends on the magnetic interaction energy in comparison to the thermal fluctuations. As demonstrated in ref. 88, 12 nm iron particles coated with polyisobutene form “string” phases due to relatively high inter-particle interaction energy:  $m^2/16\pi\mu_0a^3 \approx 15 kT$ . The same but smaller particles (10 nm in diameter) do not exhibit such structures because their energy of interaction is about one third of this value. When the particle size is increasing this leads to further increase in the magnitude of the dipolar interactions. As a result of this, the linear chains start to branch and finally a percolative, gel-like network evolves.<sup>89,90</sup> Even stronger dipolar interactions can be induced *via* application of the external magnetic field. This results in self-organization of the nanoparticles into superlattices characterized by body-centered tetragonal (bct) structures. Such superlattices have been both predicted by simulations<sup>91</sup> and observed experimentally.<sup>89</sup> During any fabrication procedure the magnetic particulate system undergoes some drying procedure. This brings additional complication as the nanoparticles can adsorb on the liquid–solid (or, sometimes, liquid–air) interface. In the former situation relatively strong attractive capillary forces arise in the menisci of the liquid between nanoparticles and can significantly modify the final morphology of the self-assembled film. In the latter case, surface tension of the liquid may have a dramatic influence on the arrangement of the nanoparticles.

Finally, spin-exchange interactions cannot be completely excluded especially in the case of existing of an intimate contact between densely packed nanoparticles. Hypothetically, such condition may be achieved on a final stage of the self-assembly process for regular arrays of monodisperse nanoparticles, or nanoparticles embedded into ferromagnetic matrix or attached to a ferromagnetic substrate. Generally, such situation is precluded due to the existence of a metal oxide or organic ligand shell interrupting (decoupling) exchange interactions between spins of the neighboring particles. However, thermal treatments (high temperature annealing) may lead to decomposition of the organic shell or/and sintering between the nanoparticles, therefore, increasing this type of magnetic interaction in the system.

### 3.2 Self-assembly on solid surfaces

Several strategies have been demonstrated for the assembly of magnetic nanostructures (Fig. 7). The relatively strong dipole

forces between the magnetic nanostructures favor their self-assembly into functional superstructures (*e.g.* linear and branched chains, close packed arrays). More importantly, the assembly is a reversible process when performed in solution (ferrofluids) enabling reversible tuning of the properties between strongly and weakly interacting regimes.<sup>92</sup> Perceivably, external magnetic field induced assembly of magnetic nanostructures has been extensively investigated. The assembly of nanomagnetic structures into macroscopic domains by self-organization has attracted significant attention which offers considerable advantages over the conventional lithographic processes.<sup>79,93–96</sup> Formation of nanostructured magnetic systems in the bottom up approach is also possible through gas phase or solution phase cluster-assembly. This topic is beyond the scope of the present review. The interested readers can be referred to one of recent reviews by Bansmann *et al.*<sup>97</sup> It was demonstrated that magnetic properties of clusters of ferromagnetic atoms are practically the same as those of magnetic nanoparticles.<sup>98</sup>

Biological systems provide excellent examples of self-assembly of magnetic nanoparticles enabling unique sense of direction with respect to geo-magnetic field. Chains of 40–100 nm magnetite nanoparticles were observed in magnetotactic bacteria. The chain-like assembly of the particles causes a permanent magnetic dipole which is critical for their orientation.<sup>99</sup> There are numerous reports describing the spontaneous assembly of ferromagnetic nanoparticles into linear and branched chains.<sup>100–102</sup> In the following discussion, we will highlight several important examples where self-assembly of magnetic nanostructures is induced by external magnetic field.

Pileni and co-workers have discussed the forces involved in the assembly of magnetic nanoparticles into chains in the presence of

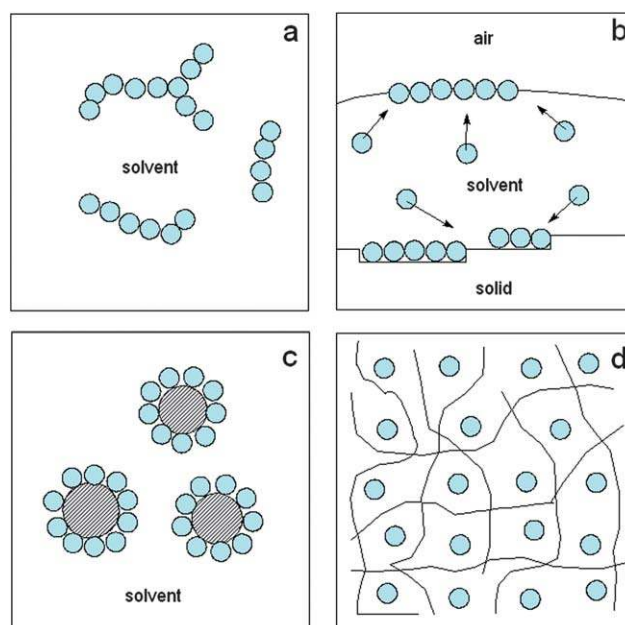


**Fig. 7** Self-assembly of magnetic nanoparticles scenario: (a) in dispersion, (b) at solid–liquid or liquid–air interfaces, (c) at nanosized objects (other colloidal particles, nanotubes *etc.*), and (d) in a solid polymer matrix during polymer synthesis or polymer-assisted self-organization due to evaporation of a solvent.

external magnetic field.<sup>79</sup> The two important forces which govern the assembly of nanoparticles are the short range van der Waals interactions and long range magnetic dipole interactions. The authors noted that the morphology of the nanoparticles assembly (belt-like or chain-like *vs.* random) is determined by the nanocrystal contact distances (Fig. 8).<sup>103</sup> Maghemite particles coated with organic ligands of different lengths (yielding different contact distances) were employed to demonstrate the transition between formation of random aggregates and chain-like structures. In particular, they have employed octanoic (C<sub>7</sub>H<sub>15</sub>COOH) and dodecanoic (C<sub>11</sub>H<sub>23</sub>COOH) acids as the organic ligands of different lengths. While dodecanoic acid coated particles exhibited random aggregation in the presence and absence of external magnetic field, octanoic acid coated particles exhibited random aggregation in the absence of external magnetic field and chain-like aggregation in the presence of external magnetic field. The authors concluded that the weak dipolar forces between the magnetic nanoparticles are insufficient to drive the self-assembly process while the van der Waals interactions when the contact distance is small (*i.e.* in the case of octanoic acid ligand), the clusters of nanoparticles are formed during solvent evaporation. The clusters, which exhibit large dipole moments, eventually organize into chain-like structures.

Singamaneni and Bliznyuk have observed the formation of chains of Ni nanoparticles as the nanoparticles solution was evaporated on silicon surface in the presence of an external magnetic field.<sup>44,26</sup> Casting the Ni nanoparticle solution in the presence of the magnetic field and subsequent solvent evaporation resulted in the spontaneous assembly of the nanoparticles into interconnected network of nanochains. It is worth noting that the absence of magnetic field during the casting and solvent evaporation resulted in isolated particles randomly distributed on the surface with no signs of aggregation. When the solvent evaporation was done in the presence of magnetic field, a size discriminative self-assembly of the particles into chains was observed. Atomic force microscopy (AFM) image in Fig. 9A shows the branched network of chains of nanoparticles with an average length of the chain between 2 and 3 μm. A careful

observation of the image also shows that all the elongated wire-like structures are actually granular in nature comprising of the individual nanoparticles (inset of Fig. 9A).

The assembly of the nanoparticles was also performed on HOPG template with atomic step edges, which can effectively act as physical confinements directing the assembly of nanochains. Fig. 9B shows a typical AFM micrograph of the nickel nanoparticles self-assembled on the surface of HOPG forming chains. It can be observed that the chains are rather straight and continuous compared to those formed on silicon substrate. It can be inferred that the nanochains follow the atomic dislocations or the so-called atomic step edges on the surface of HOPG formed during cleaving process. HOPG with atomic steps, typically 0.3–2 nm in height, acts as an excellent template resulting in a directed self-assembly or template-assisted assembly of the magnetic nanostructures. Template-assisted assembly of magnetic nanostructures is an important technique for assembly of nanostructures, which is discussed in Section 3.3.

Conversion of cobalt nanostructure to plasmonic (noble metals) nanostructures using galvanic replacement following their magnetic field induced assembly has been demonstrated by

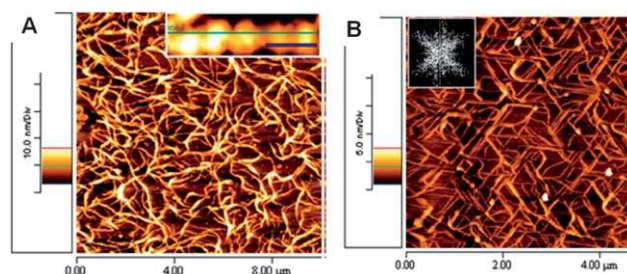


**Fig. 9** AFM topography image of self-assembled Ni nanochains formed during solvent evaporation in the presence of external magnetic field on (A) silicon substrate (inset shows the higher resolution image of a single chain showing the array of nanoparticles connected to form a chain); and (B) highly oriented pyrolytic graphite (inset: the FFT of the AFM image showing the six-fold symmetry). Reprinted from ref. 26.

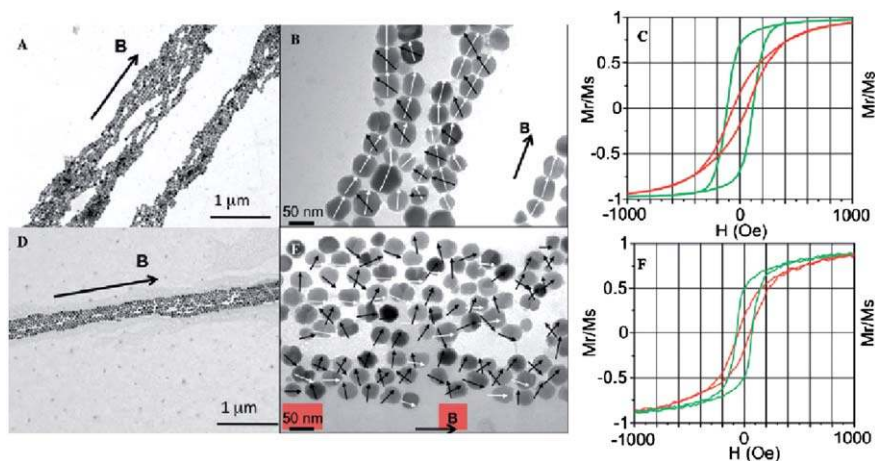


**Fig. 8** Formation of 2D belts of magnetic nanoparticles untreated (top row) and treated with a ligand (bottom row). (A) and (D) are TEM images, (B) and (E) are high resolution TEM images with arrows showing the direction of (111) crystallographic orientations (white arrows are used to indicate the case when (111) planes go parallel to the magnetic chain directions). (C) and (F) show corresponding hysteresis loops with the magnetic field applied during such measurements being either parallel (green line) or perpendicular (red line) to the direction of the nanoparticle alignment. Reprinted from ref. 95.



Zeng and co-workers.<sup>104</sup> In their approach, fabrication of chains of cobalt nanostructures was achieved by applying external magnetic field during the chemical synthesis of cobalt nanostructures. The chain structure was preserved during subsequent galvanic replacement causing chains of plasmonic nanostructures. The length of the chains of the plasmonic nanostructure governs the surface plasmon resonance of the nanoparticles chains. It was demonstrated the SPR peak could be tuned over a broad range ( $\sim 300$  nm) by controlling the strength of the external magnetic field applied during the synthesis of the cobalt nanostructures.

### 3.3 Guided and template-assisted assembly

As discussed above, template assisted fabrication of nanostructures is an attractive technique for the fabrication of magnetic nanostructures. Apart from the control over the size, shape and composition of the nanostructures, the template assisted fabrication allows the synthesis of pre-assembled structures, for example, vertically aligned nanorods in the case of AAO and parallel arrays of nanowires in the case of HOPG templates. Physical and chemical templates can also be employed to assemble chemically synthesized magnetic nanostructures from solution. The templates can be grown by both top-down (e.g. lithographic approaches to form periodic pits, pores, grooves, posts) and bottom-up (e.g. self-assembly of block copolymers) approaches. Below we discuss some recent examples involving the assembly of magnetic nanostructures using template-assisted approach.

Park and co-workers have demonstrated a universal approach for the assembly of wide variety of nanostructures (magnetic, noble metals and semiconducting) into chains.<sup>105</sup> Their approach relies on using mussel-inspired polymeric template for the assembly of the nanostructures into chains. More specifically, an anionic glycosaminoglycan, hyaluronic acid (HA), was used as a macromolecular template, and catechol (with enediol functional group), which serves as adherent species, was chemically introduced onto the backbone of the HA. The bioinspired macromolecular template, enabled the assembly of magnetic nanoparticles into chains. Fig. 10A shows the TEM image of  $\text{Fe}_3\text{O}_4$  nanoparticles assembled into chains. The authors employed vibrating-sample-magnetometer to reveal a significant increase in the coercivity of the assembled  $\text{Fe}_3\text{O}_4$  nanoparticles from 35.2 Oe to 48.7 Oe due to the coupling of magnetic dipole moments along the chain of  $\text{Fe}_3\text{O}_4$  nanoparticles (see Fig. 10B). It was also demonstrated that the length of the chain assembly could be tuned using hyaluronic acid-graft-catechol templates with various contour lengths.

Sibener *et al.* have reported the assembly of FePt nanoparticles using phase separated block copolymers as physical template.<sup>106</sup> It is known that block copolymers phase separate into wide variety of patterns with nanoscale periodic structures. They used polystyrene (PS)/poly(methyl methacrylate) (PMMA): PS-*b*-PMMA diblock-copolymer thin film, which was irradiated with vacuum ultraviolet light to selectively etch PMMA domains at the surface to selectively etch the PMMA cylinders. Etching the PMMA domains resulted in periodic grooves in the polymer film. The corrugated film was used as a template for the self-assembly of oleic acid-capped FePt nanocrystals. It was found that the

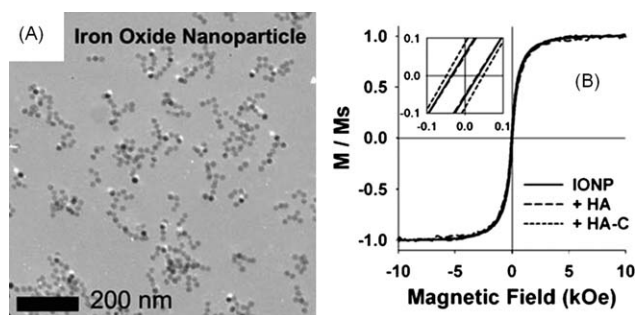


**Fig. 10** (A) TEM imaging showing the bio-inspired approach for the assembly of iron oxide nanoparticles into linear chains, (B) magnetism of  $\text{Fe}_3\text{O}_4$  nanoparticles (solid line), mixture of iron oxide nanoparticles and hyaluronic acid (long dashed line), and iron oxide nanoparticles assembly (short dashed line). Reprinted from ref. 105.

FePt nanoparticles selectively adsorb (nearly 100%) within the photochemically created nanoscopic channels.

Yet another method of assembling magnetic nanoparticles using block-copolymers as template was demonstrated by Takahashi and co-workers.<sup>107</sup> They have shown the self-assembly of magnetic nanoparticles by combining chemically synthesized  $\text{Fe}_3\text{O}_4$  nanoparticles with a diblock copolymer comprised of PS and PMMA. The block copolymer based upon its composition self-assembled to form periodic array of PS dots in PMMA matrix. Volume fraction of the  $\text{Fe}_3\text{O}_4$  suspending solution and the withdrawal speed of the template exhibited a dramatic influence on the formation of array of magnetic nanostructures. It was found that periodic array of magnetic nanostructures with one or multiple nanoparticles adhered to the PS domain was possible for small volume fraction of the nanoparticles and low withdrawal speed. Specifically, below a withdrawal speed of  $0.5 \text{ mm s}^{-1}$  and a nanoparticle volume fraction of less than 0.01 vol%, the selective deposition of one to several nanoparticles on every single PS dot was observed.

Cobalt nanoparticle arrays were formed by annealing Co film deposited on topographically patterned silicon substrates.<sup>108</sup> Upon annealing the Co film, the film dewetted to form Co nanoparticle which self-assembles obeying the physical confinement of the substrate. The Si surface was pre-patterned with an array of 200 nm period pits, which host one Co nanoparticle upon annealing 15 nm thick Co film at  $850^\circ\text{C}$ . The authors noted that the Co nanoparticle size and uniformity are governed by the initial film thickness, annealing temperature, and template geometry. In a related method, which involved laser annealing, dewetting of 5 nm film gave one particle per cavity. It is also interesting to note that the Co nanoparticles were comprised of predominantly twinned fcc crystals with weak magnetic anisotropy although the pristine Co films exhibited a mixture of hcp and fcc phases.

### 3.5 Layer by layer assembly

Yet another important approach for realizing highly organized (or vertically stratified) magnetic nanostructures is using layer by layer (LbL) assembly. LbL assembly involves alternate adsorption of the complementary species with specific interaction such as electrostatic, hydrogen bonding or biorecognition. LbL has



been extensively applied in the fabrication for the polyelectrolyte multilayers involving electrostatic interactions between alternating cationic and anionic polyelectrolytes.<sup>109</sup> Apart from pure polymeric components, numerous nanostructured materials such as metal nanostructures, semi-conducting quantum dots, carbon nanotubes, inorganic clays have been successfully incorporated to realize multi-functional materials. Of particular interest in the context of present review is the incorporation of magnetic nanostructures into LbL assembled polymer composites and LbL approach as directly applied to magnetic nanoparticles.

In one of the early studies, Kotov and co-workers have demonstrated the incorporation of naked and silica coated  $\text{Fe}_3\text{O}_4$  nanoparticles into polyelectrolyte multilayers assembled on flexible plastic substrates.<sup>110</sup> The multilayers were comprised of poly(diallyldimethylammonium bromide) (PDDA) and  $\text{Fe}_3\text{O}_4$  nanoparticles. The multilayered films exhibited excellent mechanical properties and adhesion to the substrate with no signs of cracks or delamination even under large strains. The authors noted that apart from the relative simplicity such multilayered magnetic nanoparticle films offer unique advantages compared to magnetic layers obtained using vacuum deposition methods in that the technique provides a much better control over the structure of individual grains. Furthermore, the authors also demonstrated a drastic reduction of the cooperative magnetization switching between adjacent magnetic nanoparticles due to the presence of the insulating silica shell. Such organic/inorganic non-magnetic layers acting as precise spacer between the magnetic nanoparticles can be employed to fine-tune the inter-particle or inter-layer magnetic interaction.

Using a similar approach, Lvov and co-workers have fabricated multi-functional microcantilevers based on multilayered nanocomposite.<sup>111</sup> The multilayered nanocomposite was comprised of PDDA, nanoclay (montmorillonite) and magnetite nanoparticles. While the PDDA and nanoclay provide the structural integrity, the magnetic nanoparticles in the nanocomposite enabled the release of the patterned nanocomposite layer from the substrate resulting in free standing cantilever. In a different approach, LbL has been used directly to assemble  $\text{Fe}_3\text{O}_4$  nanoparticles.<sup>112</sup> Assembly of nanostructures was achieved by a combination of electrostatic (capped with different ligands providing opposite surface charge) and magnetic interactions (external magnetic field during adsorption). The effect of the external magnetic field on assembly of nanoparticles was evidenced by increased electronic absorption in the case of external magnetic field-assisted films. Magnetic force microscopy was also employed to reveal the higher degree of ordering in such nanoparticle superstructures compared to those assembled using only electrostatic interactions.

#### 4. Morphological features of self-assembled arrays of magnetic nanoparticles

Highly directional magnetostatic dipole–dipole interactions cause formation of characteristic 1D nanostructures—nanochains already in nanoparticle dispersion. Such dipolar chains were predicted by Monte Carlo simulations.<sup>113–115</sup> When the nanoparticles are transferred onto a solid substrate from such dispersions two basic morphologies are possible: nanochains and nanorings (Fig. 11).<sup>116</sup> The latter type of the morphology is often

considered to be a result of degradation of the dipolar chains. Formation of nanochains of ferromagnetic and superparamagnetic nanoparticles on solid substrates or directly in liquid dispersions was experimentally observed by many authors.<sup>86,102,117–120</sup> The particles under study had very different nature: magnetite, cobalt, nickel, Ni–Co alloys, core–shell structures like silica or polymer coated ferromagnets. Interestingly enough similar nanostructures were observed in materials traditionally considered to be nonmagnetic (Ag, Au).<sup>119</sup>

Chu *et al.* reported on the genesis of the nanostructure growth during fabrication of films *via* casting of nanoparticle dispersions on a solid substrate following by solvent evaporation.<sup>121</sup> Variation of the initial concentration of the dispersion caused dramatic changes of the final nano-architecture. When the magnetic nanoparticle concentration was low several micron long straight rods were formed. Increase of the concentration promoted formation well-ordered nanostructures—snowflake fractals (Fig. 12). The authors believe that both magnetostatic interactions between  $\text{Fe}_3\text{O}_4$  cores and van der Waals interactions between capping molecules (vinyl pyrrolidone or oleic acid) were responsible for the final dendritic structures. Different nanostructures were also observed depending on the temperature of solvent evaporation. Application of an elevated temperature (above 150 °C) promoted formation of the nanostructures while when the temperature was below this value no highly branched nanostructures could be formed.

In another study, silica shell was created on weak magnetic iron oxide nanoparticles *via* sol–gel technology.<sup>122</sup> The thickness of the silica shell was controlled (from 14 to 32 nm with the magnetic core size of ~78 nm) during the synthesis by varying the concentration of silica precursor—tetraethylorthosilicate (TEOS). Therefore the degree of magnetostatic interaction was varied. Transmission electron microscopy revealed that magnetic nanoparticles are regularly embedded in the continuous silica shells which are formed along one-dimensional wires. The

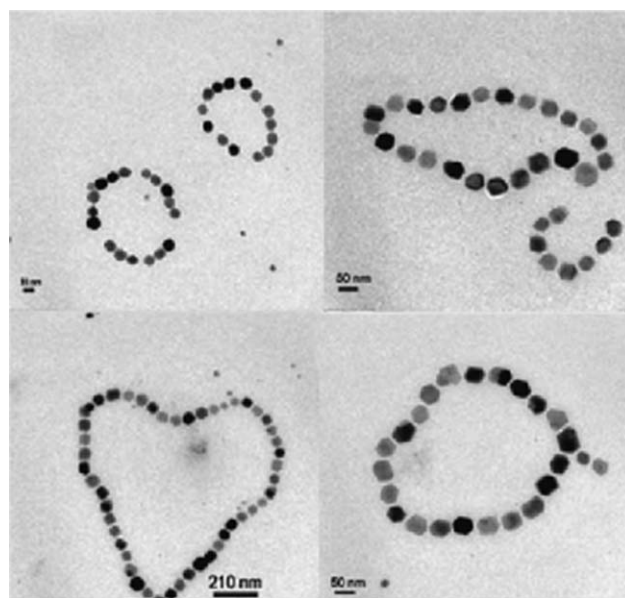


Fig. 11 Necklace-like nanoarrays of magnetic nanoparticles. Reprinted from ref. 116.



**Fig. 12** SEM image of a 3D dendritic morphology formed under self-assembly of  $\text{Fe}_2\text{O}_3$  with application of pyrrolidone as a ligand at  $200^\circ\text{C}$ . Reprinted from ref. 121.

observed wormlike morphology of the nanostructures demonstrated that the weakly ferromagnetic nanoparticles self-assemble into 1D particle chains already in the dispersion (Fig. 13). The authors concluded that formation of such chains was due to magnetic dipolar interaction between the weakly ferromagnetic nanoparticles, which favored their head-to-tail orientation.

Variation of the observed morphology was studied depending on the preparation conditions. Particularly, the amplitude of ultra-sonication applied for better dispersion of the nanoparticles had great impact on the morphology of the resultant products. As the amplitude of ultra-sonication increased from 20% to 40% and then 60%, long and highly branched wires became progressively shorter and without branching. In addition more isotropic shorter chains were formed during self-assembly without application of an external magnetic field while highly anisotropic (along the field) longer chains were formed if the magnetic field was applied.

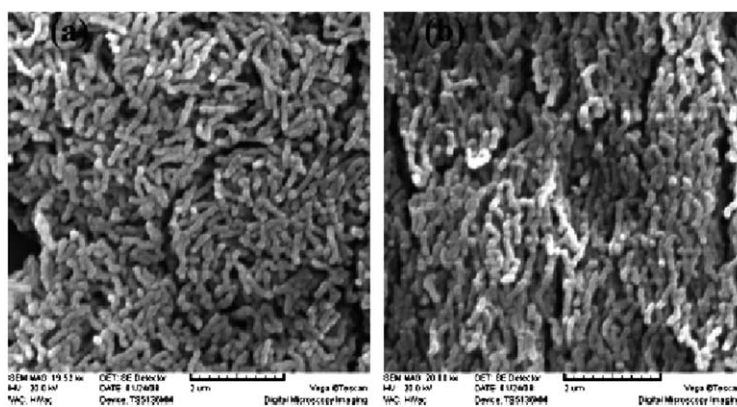
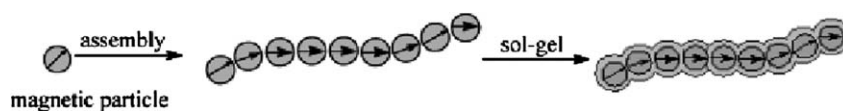


**Fig. 13** (Top) Formation of 1D magnetic nanochains followed by their encapsulation through a sol-gel process and (Bottom) SEM images of such structures cast on a solid glass substrate from ethanol without an applied magnetic field (left) and under applied magnetic field (right). Reprinted from ref. 122.

Ozdemir *et al.* studied self-assembly of magnetic  $\text{Fe}_3\text{O}_4$  nanoparticles with an average size of 6 nm under an influence of enhanced magnetic force.<sup>123</sup> The authors reported on formation of unique micrometre-sized morphologies achieved in the route of self-organization of sub-micrometre size magnetic beads having metallic nanoparticles imbedded into a polymer matrix. Some exotic nanostructures were formed in the presence of the external magnetic field on a patterned solid surface upon solvent evaporation. The authors claim that the combined effect of magnetic field and evaporation rate might help the control of nanoparticle behavior on surfaces and interfaces in constructing of hierarchical supramolecular structures (Fig. 14).

Influence of alternating magnetic field on the morphology of self-assembled magnetic nanoparticles was reported in ref. 124.  $\text{Fe}_3\text{O}_4$  nanoparticles with the diameter of 10–11 nm were in superparamagnetic state at room temperature. In the absence of any magnetic field, nanoparticles formed amorphous aggregates on a solid substrate after solvent evaporation. On contrary, fibrous assemblies were formed when 50 Hz alternating magnetic field was applied either in plane of the film or along the substrate normal during solvent evaporation. In the case of the field vector

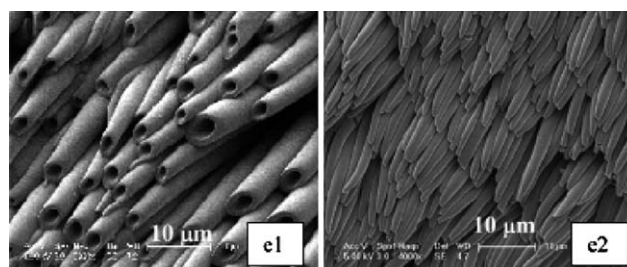


**Fig. 14** Self-assembly of polymer magnetic beads (*i.e.*, magnetic nanoparticles encapsulated into polymer) depending on the combination of casting conditions (solvent, substrate and external magnetic field). Reprinted from ref. 123.

applied normal to the film surface the width of the assemblies decreased from  $\sim 2$  mm to  $\sim 1$  mm and their length increased from 34 mm to more than 70 mm when the field strength increased from 10 to 72 kA m $^{-1}$ . When the alternating magnetic field was applied parallel to the film surface very long ( $\sim 250$  mm) chains were formed, and both the length and the width of aggregates were increasing with the field strength (Fig. 15). The difference in morphology is explained by the authors by different arrangements of the magnetic dipole moments in neighboring nanoparticles constituting the chains: in-plane magnetic field promoted head-to-tail assembly of the dipoles, while perpendicular field caused the same dipoles to obey more energetically favorable anti-parallel arrangement.

More regular 2D supercrystals are formed with smaller nanoparticle of magnetic materials. Krishnan *et al.* have systematically studied self-assembly behavior of Co nanoparticles with the size slightly below or slightly above the superparamagnetic limit  $D_{sp}$  depending on particle size and shape (spheres or disks).<sup>9</sup> Because of very small particle size magnetostatic interactions were weak and comparable with other interactions. Therefore a combination of competing weak forces (steric, van der Waals, entropy and magnetostatic) governed the self-assembly process and determined the resulting structural organization in the system. The authors demonstrated the possibility of directed formation of regular 2D crystals with square or hexagonal close packing.<sup>125</sup> A 2D arrangement with a square unit cell was observed for smaller nanoparticles (Fig. 16A). This behavior of nanoparticles can be understood as an arrangement, which corresponds to minimized steric repulsive

forces between the surfactant molecules on their surface. The nanoparticles were coated with an organic surfactant monolayer due to the applied synthetic procedure. Because of small particle size ( $\sim 5$  nm) the fraction of surface atoms constitute almost 50% of the total Co atoms and therefore, the interaction of the surfactant chain on the surface significantly affects the organization behavior of these nanoparticles. As the particle size increased, the contribution from the surface atoms becomes less dominating. This leads to a hard-sphere type behavior and 2D square lattice is replaced with more closely packed 2D hexagonal arrangement (Fig. 16A). When two different sizes of Co nanoparticles were mixed to give a bimodal-size distribution interesting new nanostructures with a superlattice of bigger particles each of them surrounded with several smaller ones have been observed. The formation of such structure can be driven by entropy forces. A preferential wetting of the surface by the larger particles leads to a depletion zone around them, which can be occupied by smaller size particles as has been theoretically predicted for soft materials.<sup>126</sup> When the particle size increases over  $D_{sp}$  limit (10 nm for Co), the magnetostatic interactions dominate the self-assembly process. Therefore, linear chains or loops are formed instead of regular 2D arrays.

For non-spherical nano-disk shapes, liquid-crystal-like arrays with increased orientation order as a function of concentration were observed (Fig. 16B). Such arrangement of nanoparticles is driven by strong hydrophobic interaction between surfactant tails. Nanodisks are prone to stack face to face in order to maximize contact between the surfactant tails. Such face to face placement of anisotropic shape nanoparticles along chains (with presumably anti-parallel arrangement of neighboring magnetic dipole moments) is favorable also from the viewpoint of magnetostatic energy minimization.

3D self-assembly is also possible in a similar fashion. The general requirement to the nanoparticles is their relatively small size (and therefore stronger coupling between spins) and narrow size distribution. Pileni and co-workers have made a pioneering study in the field. Depending on the preparation conditions long-range order 2D or 3D supra-crystals with face-centered cubic (fcc) symmetry or disordered aggregates were fabricated from 7.5 nm Co nanoparticles.<sup>127–129</sup> The 3D assemblies with the

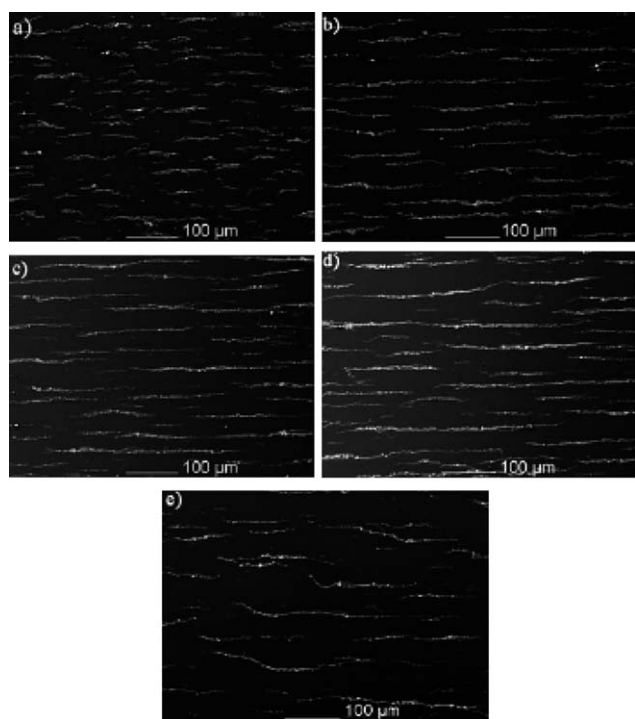


**Fig. 15** SEM images of highly anisotropic assemblies of Fe $_3$ O $_4$  nanoparticles formed in the presence of a parallel-applied alternating magnetic field (the field intensities are  $\sim 11$ ,  $\sim 25$ ,  $\sim 45$ , 60 and 72 kA m $^{-1}$  when going from (a) to (e)). Reprinted from ref. 124.

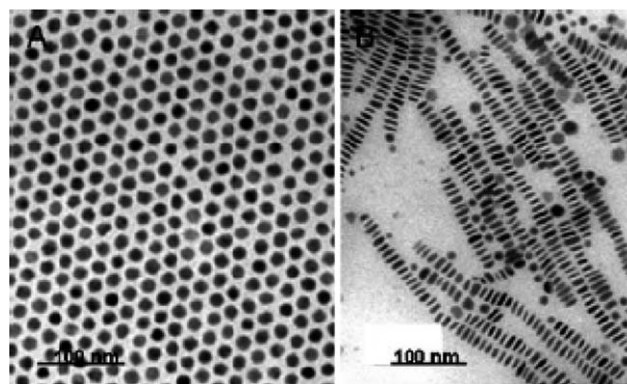


**Fig. 16** Examples of regular patterns formed during self-assembly of magnetic nanoparticles: 2D hexagonal array of 10 nm magnetic nanospheres (A) and 1D stacks of 5  $\times$  20 nm anisotropic nanodisks (B). Reprinted from ref. 9.



mesoscopic order (intermediate between the atomic level and the bulk state) have the potential to exhibit many interesting new properties. HOPG was used as template in these studies. To form the disordered amorphous-like assemblies the solvent (hexane) evaporation was performed relatively fast (12 hours) under a nitrogen flow saturated with hexane at 7 °C. The ordered structures were obtained when the solvent evaporation took place at room temperature under nitrogen in almost completely isolated system saturated with hexane such that evaporation took in total 72 hours.

Narrow-size distribution magnetic nanoparticle can be grown with application of bioengineering approach<sup>64,130</sup> when apoferritin, a cage-like protein, is applied as a temporary template. Because of high size uniformity the Fe<sub>3</sub>O<sub>4</sub>-γ-Fe<sub>2</sub>O<sub>3</sub> nanoparticles grown by this approach can easily self-assemble into large (hundreds of micrometre size) mesoscopic three-dimensional (3D) face-centered cubic (fcc) crystals (Fig. 17). In such crystals nanoparticles are acting as the crystal's "atoms" giving the material unique ferromagnetic properties.<sup>130-132</sup> In more concentrated magnetic nanocrystal systems, exchange interactions are induced which have a significant effect on the magnetic behavior. It has been shown that these interactions lead to spin-glass-like behavior as observed in traditional ferromagnetic systems where magnetic atoms interact *via* long-range Ruderman–Kittel–Kasuya–Yosida (RKKY) interaction forces.<sup>133-135</sup>

## 5. Magnetic properties of nanoparticle arrays

### 5.1 Magnetometry

Magnetic nanoparticle arrays fabricated through thin film deposition techniques, thin film self-assembly, or physical nanocluster deposition techniques have in common that they typically contain small amounts of magnetic materials resulting

in a low total magnetic moment, respectively.<sup>136</sup> Hence, magnetic characterization can be a significant challenge. This holds in particular when integral methodologies of measurement are applied and signal contributions from substrate materials have to be taken into account. One has to remember that every material has some form of magnetic response. Even substrates free from magnetic impurities will have a diamagnetic field-induced signal which can easily dominate the sample signal of magnetic nanoparticles. For instance, a clean sapphire substrate has a diamagnetic, magnetic susceptibility at room temperature of about  $\chi = -4.4 \times 10^{-9} \text{ m}^3 \text{ kg}^{-1}$ .<sup>137</sup> For a substrate of 0.5 mm thickness and a surface area of 25 mm<sup>2</sup> a field of 1 T gives rise to a negative field-induced magnetic moment exceeding absolute values of  $2 \times 10^{-5} \text{ emu} = 2 \times 10^{-8} \text{ Am}^2$ .<sup>138</sup> While diamagnetic signals at constant temperature are linear in the applied field and correction of the data can be done rather easily, the situation becomes more complex when temperature dependent investigations are undertaken and the temperature dependence of the substrate signal has to be taken into account. The latter typically superimposes the potentially unknown temperature dependence of the sample magnetic moment.

With these issues in mind one can group the magnetic characterizations into two classes: those that are integral and include the substrate magnetic signal and those that are specific to just the contribution from the nanoparticles. Such specificity can be achieved by scanning probe methodologies or element specific spectroscopies such as X-ray magnetic circular and linear dichroism. Next we will focus on the integral methods which are far more frequently used and have the advantage that they are inherently quantitative methods.

Modern integral magnetometry methodologies exploit ac and dc approaches. Extensively used today are vibrating sample magnetometers and, with increasing popularity, superconducting quantum interference devices (SQUID).<sup>139,140</sup> The latter show the highest sensitivity by taking advantage of the steep

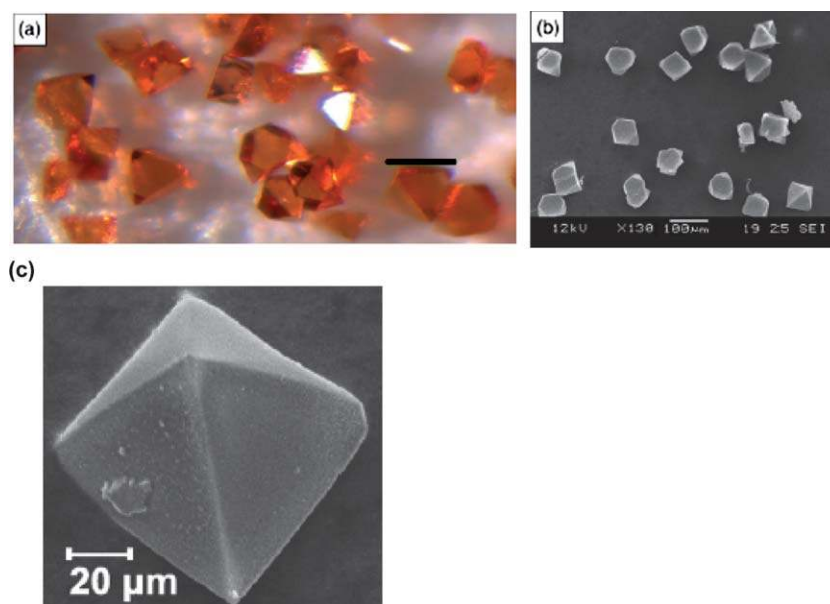


**Fig. 17** Optical (a) and SEM (b and c) images of 3D fcc crystals using "bioengineered" magnetic nanoparticles of Fe<sub>3</sub>O<sub>4</sub>-γ-Fe<sub>2</sub>O<sub>3</sub> (magnetoferritin) of 8 nm (a and b) and 6.5 nm diameter as constituting "atoms". Scale bar for images (a) and (b) is 100 μm. Reprinted from ref. 64 and 130.



characteristics of the penetrating magnetic flux *vs.* external magnetic flux applied to the superconducting ring which is the center piece of the SQUID magnetometer. Here the field induced supercurrent has to tunnel through a weak link in accordance with the DC Josephson effect thus creating the superior sensitivity on flux changes caused by the stray-field of the sample.<sup>141</sup> Conservative estimates shows that SQUIDs allow detecting minimal moments as low as  $10^{-10}$  emu =  $10^{-13}$  Am<sup>2</sup>.

For comparison, an individual  $\gamma$ -Fe<sub>2</sub>O<sub>3</sub> nanoparticle of about 12 nm diameter has a moment of about  $3 \times 10^{-19}$  Am<sup>2</sup> making an ensemble of a few hundred thousands of individual particles easily detectable.<sup>142</sup> Modern SQUIDs such as the commercial MPMS (Quantum Design) provide push-button and state-of-the-art temperature and magnetic field control.<sup>143</sup> Recently, the technological boundaries of SQUID magnetometry have been pushed further motivated by the application for measurements on nanoscale magnets where not only sensitivity is of importance but at the same time high gain, wide bandwidth and low back-action are desirable.<sup>144</sup>

## 5.2 SQUID magnetometry in magnetic nanoparticle characterization

Integral SQUID magnetometry has been extensively used for the magnetic characterization of magnetic nanoparticles and most likely will continue so in the future. Fig. 18 shows a prototypical magnetometric investigation of nearly interaction free  $\gamma$ -Fe<sub>2</sub>O<sub>3</sub> nanoparticles which have been randomly dispersed in a polystyrene matrix.<sup>142</sup> The particles were produced by a synthetic strategy, more specifically, *via* thermal decomposition of metal carbonyls in the presence of appropriate surfactants.<sup>82,145,146</sup> The procedure is known to result in highly uniform nanoparticles. The individual particles in these 3D samples have a mean diameter of 11.6 nm. The Fig. 18a–c show the temperature dependence of the magnetic moment, *m*, after zero-field cooling (ZFC) the sample and measuring the temperature dependent magnetic moment, *m vs. T*, on field heating (FH) in an applied

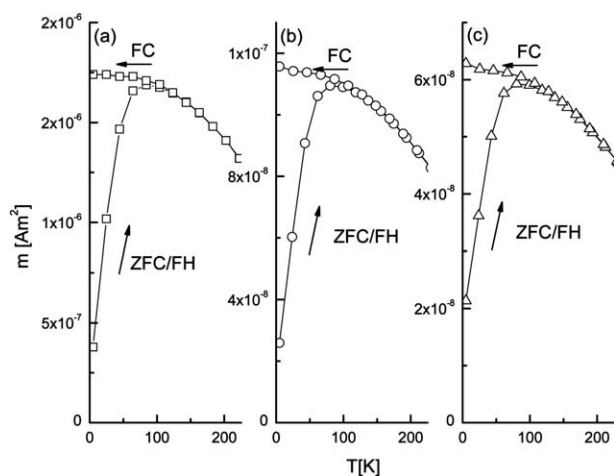


**Fig. 18** Temperature dependence of the respective magnetic moment, *m*, of  $\gamma$ -Fe<sub>2</sub>O<sub>3</sub> samples with decreasing number of dispersed nanoparticles  $2.88 \times 10^{13}$  (a),  $1.5 \times 10^{13}$  (b), and  $7.8 \times 10^{12}$  (c). After zero-field cooling the samples, *m vs. T* has been measured on heating in an applied field of 25 mT. Subsequent field-cooling curves indicate the onset of a non-equilibrium regime below the blocking temperature.

field of 25 mT. The subsequent field-cooling curve (FC), splits off from the ZFC/FH branch at the blocking temperature as outlined in Section 1 where the mechanism of superparamagnetic blocking has been introduced in detail. The samples creating the *m vs. T* data shown in Fig. 18 differ in their respective density of dispersed nanoparticles according to  $2.88 \times 10^{13}$  (a),  $1.5 \times 10^{13}$  (b), and  $7.8 \times 10^{12}$  (c) individual nanoparticles.<sup>142</sup> From measurements like these ZFC/FH and FC *m vs. T* curves together with magnetic isothermal *m vs. H* measurements and the investigation of thermoremanent magnetization one can determine information such as the nanoparticle number, the moment per particle, and some qualitative estimates of the anisotropy energy which determines the blocking temperature of the nanoparticle ensemble.

Next we briefly outline how one can determine both particle number and moment per particle from isotherms *m vs. H*. For simplicity we assume nanoparticle ensembles with negligible magnetic anisotropy such that the classical limit of a Langevin description is an appropriate approximation, and a narrow particle size distribution such that each individual particle moment is in good approximation given by the distribution averaged value *m*<sub>0</sub>. We express the total magnetic moment as *m*(*H*, *T*) = *Nm*<sub>0</sub>*L*(*m*<sub>0</sub>*μ*<sub>0</sub>*H*/*k*<sub>B</sub>*T*) where *N* is the number of particles and *L* is the Langevin function. Using a device such as a SQUID magnetometer one measures the integral magnetic moment *m* of a sample. It is straightforward to see that an isothermal measurement *m vs. H* in the limit of virtual saturation achieved for *m*<sub>0</sub>*μ*<sub>0</sub>*H* ≫ *k*<sub>B</sub>*T* yields the saturation value *Nm*<sub>0</sub>. Of course it is best practice to determine the saturation value at various temperatures and perform a limiting extrapolation *T* > 0 for most accurate values of *Nm*<sub>0</sub>. Next one explores isotherms at *T* > *T*<sub>b</sub> in the limit *m*<sub>0</sub>*μ*<sub>0</sub>*H* ≪ *k*<sub>B</sub>*T*. Here the Langevin function like all Brillouin functions can be linearized. The slope of the isotherms in the linear regime is given by  $\partial m / \partial H = Nm_0^2 \mu_0 / (3k_B T)$ . With both *Nm*<sub>0</sub> and *Nm*<sub>0</sub><sup>2</sup> experimentally accessible one can determine *N* and *m*<sub>0</sub> separately. Of course, with access to numerical non-linear least squares fitting algorithms, both parameters can be easily determined from a non-linear two parameter fit of an isotherm or better a set of isotherms.

In Fig. 18 we see that, qualitatively and despite the fact that the density of nanoparticles varies between samples (a), (b), and (c), the blocking temperature remains constant and the FC branch separates horizontally from the ZFC/FH branch. This FH/FC-behavior indicates in first approximation absence of particle-particle interaction. However, it is the strength of the ultra-precise SQUID methodology to detect even the smallest corrections to the idealized case of non-interacting magnetic nanoparticles. As outlined above, there is always some degree of interaction present. In the absence of exchange there must remain the long-range dipolar interaction in the hierarchy of magnetic interactions Ref. 142 outlines in detail how those extremely weak interactions give rise to small deviations from the classical Langevin-behavior. Moreover, the long-range nature of the dipolar interaction gives rise to subtle deviations from conventional extensive thermodynamics. Such deviations are of fundamental importance for progress in our understanding of thermodynamics and have been evidenced for the first time experimentally in magnetic nanoparticle ensembles with the help of scaling analysis.<sup>126</sup>

More generally, interactions in magnetic nanoparticle systems became a fascinating subject in recent years. Less exotic than the subtle effect of nonextensive thermodynamic behavior but intriguingly nevertheless is the fact that almost all types of magnetic long-range order and interaction-controlled phenomena known from atomic bulk systems have found a counterpart in magnetic nanoparticle systems where the atomic moments have been replaced by superspins. A pioneering work in this regard has been done on interacting ferromagnetic CoFe-nanoparticles embedded in a sapphire matrix in the form of discontinuous multilayers.<sup>147</sup> A series of interaction induced ordering phenomena from superspin glass to reentrant superferromagnetism has been reported.<sup>147</sup> Subsequent detailed investigations including dynamic ac susceptibility measurements as a function of temperature, frequency and field amplitude together with element specific imaging techniques such as X-ray photoemission electron microscopy (PEEM) and also magneto-optical Kerr microscopy were able to prove the existence of such long-range ordered states in superspin nanoparticle ensembles.<sup>148–152</sup>

Origins of the interaction between the nanoparticles are as diverse as the various forms of magnetic order and not always easy to discriminate. Likewise the identification of a long-range ordered phase is a subtle task as is its discrimination from local short range order. As an example for the latter, which can easily be confused with a domain state of a long range ordered thermodynamic equilibrium phase, serves the toy model of magnetostatically interacting compass needles on a square lattice with  $XY$ -degrees of freedom. The latter is often but misleadingly used to demonstrate ferromagnetic Weiss regions of spontaneous ferromagnetic order. The presence of short range ordered domains is, however, not sufficient to evidence spontaneous ferromagnetic order. Even more involved, the identification of a true thermodynamic superspin glass phase requires evidence *via* an arsenal of typical spin glass criteria such as spin glass dynamics with its characteristic slowing down on approaching the glass temperature, aging, re-juvenation and memory effects in order to make a convincing case.

Magnetic interactions, which are at the origin of magnetic order and equilibrium magnetic phase formation, range from the always present dipolar interaction discussed above over conventional quantum mechanical exchange for nanoparticles in close proximity to indirect exchange when the particles loose contact. RKKY-type interaction can be found when the particles are embedded in a conducting matrix and even exotic quantum tunneling mediated exchange has been reported.<sup>150–155</sup> The investigation of the impact of dimension and symmetry of magnetic interaction on the universality of possible thermodynamic phase transitions is the domain of the theory of phase transitions and critical phenomena.<sup>156,157</sup> Here, a breathtaking bulk of work has been produced with deep insights into the fundamental aspects of statistical physics.<sup>158</sup> In the case of interaction sufficiently short in range there are rigorous results one can rely on such as the celebrated Mermin–Wagner theorem predicting the absence of long-range order in the case of ferromagnetic or antiferromagnetic interaction in two dimensions for continuous Heisenberg symmetry in contrast to Onsager's celebrated proof of critical behavior in two dimensions in the case of Ising-symmetry.<sup>159,160</sup> While there is rigorous ground for the case

of short range interaction the situation is far more controversial and involved when long-range magnetostatic interactions are involved.<sup>161</sup> Here experiments play a leading role to allow further advances in theoretical insights.<sup>162</sup>

Micromagnetic simulations are an important tool to incorporate the effects of dipolar interaction into the theoretical interpretation. A sometime important detail can be found in the fact that magnetic nanoparticles cannot always be considered to be perfect spheres with homogeneous magnetization. As a result, the approximation of the magnetic stray-field of a nanoparticle *via* an individual magnetic dipole may be an oversimplification and multipole effects can be of importance adding significant complexity to the already hard problem of long range magnetostatic interaction.

The magnetic structure of nanoparticles can be complex even for single domain particles. Nanoparticles often show a chemical core/shell structure with potential significant implications for their magnetic properties. The most prominent and frequently studied effect in core/shell magnetic nanoparticles is the presence of an antiferromagnetic shell of an otherwise ferromagnetic nanoparticle. Here the effect of exchange bias can be observed. In fact, it was in Co/CoO core-shell nanoparticles where Meiklejohn and Bean first discovered the exchange bias phenomenon.<sup>163,164</sup> The latter core-shell structure forms naturally when exposing the ferromagnetic Co particles to atmosphere where a passivation shell of a few nm forms with antiferromagnetic properties. The antiferromagnetic shell acts as a magnetic pinning component for the ferromagnetic core which, as a result, experiences an exchange induced unidirectional anisotropy breaking the symmetry of the magnetization reversal with respect to the applied magnetic field. The dynamic hysteresis of the magnetic nanoparticle ensemble is therefore shifted along the magnetic field axis by the exchange bias field. At the same time the overall dynamic coercivity can be enhanced. Similarly, magnetic nano-precipitates, *e.g.*, ferromagnetic nanodroplets and antiferromagnetic host matrix show these exchange bias effects with an additional typical exchange bias phenomenon known as training effect.<sup>164,165</sup> Here the magnetization reversal of the nanodroplets triggers spin-configurational changes in the antiferromagnetic host matrix. The resulting successive reduction of the exchange bias field (training effect) has been successfully described through a discretized Landau–Khalatnikov relaxation approach.<sup>166–168</sup>

### 5.3 Magnetic force microscopy

Scanning probe microscopy, which includes a wide variety of techniques, involves a sharp probe (usually with nanoscale dimensions) which interacts with the substrate. Physical quantities such as force, current, capacitance, conductivity are employed to unveil the structure and/or properties of surface under investigation with unprecedented resolution.<sup>169–173</sup> Magnetic force microscopy (MFM), which belongs to a broad category of scanning probe microscopy is similar to electrostatic force microscopy except that the tip interacts with the magnetic stray fields created by the magnetic domains of the sample, as opposed to the electrostatic surface potential.

MFM operates in the non-contact mode, in which a tip coated with a ferromagnetic material (such as Ni, Co, Fe) detects the

stray magnetostatic field of the magnetic dipoles of the sample.<sup>174,175</sup> As the magnetostatic interactions are long-range (similar to the electrostatic interactions), the magnetic imaging is performed between the probe and surface at a set distance, typically 20–50 nm, in a mode commonly referred to as lift-mode. Lift-mode involves a special raster scan where each line is scanned twice before the next line is scanned. In the first line scan, the topography is scanned in a conventional manner and surface profile is stored. Then the probe is lifted by a set amount (several-tens nanometres) and the probe retraces the previous topographic line scan. During the second line scan the cantilever deflection is monitored and used to create the MFM image. MFM has been widely employed to probe magnetic recording media and to image and record the magnetization of Co, Ni, and Fe magnetic micro- and nanostructures down to a single nanodot.<sup>26,176–179</sup>

MFM has been extensively used to probe the magnetic microstructure and/or estimation of magnetic moment of a wide variety of magnetic materials including magnetic recording media, Co nanoparticles, Co nanowires iron nanoparticles, Ni–Cu barcodes, and magnetotactic bacteria.<sup>176,178–181</sup> Resolution of the magnetic force microscopy is dependent upon several factors such as size and shape of the tip, tip–sample distance, noise and sensitivity of the instrument. As in conventional imaging modes (contact mode and tapping mode imaging), the vertical resolution is governed by the ambient (electrical, mechanical and acoustic) noise, while the lateral resolution is governed by the above mentioned parameters. Tip sharpness is an extremely important factor, which governs the best lateral resolution that can be achieved with sharper probes enabling higher resolution. For larger tip–sample separations, the stray field experienced by the magnetic tip is small resulting in poor signal and hence poor lateral resolution. On the other hand, higher resolution can be achieved for small tip–sample separations (lift heights). It is also important to ensure sufficient lift-height to eliminate contribution from van der Waals interactions.

In a very recent study, Neves and co-workers have compared the response of lift mode MFM to non-magnetic and magnetic nanoparticles.<sup>182</sup> Interestingly, the authors noted magnetic tip response (phase shift) that might be mistaken for a magnetic interaction from even non-magnetic nanoparticles. They noted that such a response is inherent to MFM technique and therefore could also be detected from individual superparamagnetic nanoparticles with diameter <10 nm, whose field is too weak to be detected. Positive phase shifts, which are indicative of repulsive interactions were observed in the case of the non-magnetic interactions. On the other hand, in the case of magnetic nanoparticles, mostly negative phase shifts were observed at the center of the particles while positive responses only at the edges. The authors noted that the difference in phase shift response can be used to characterize the nature of the interactions, and thus the magnetic properties of the surface features. Their study also clearly underscores that with careful analysis of the MFM images, it can clearly discriminate between magnetic and nonmagnetic nanoparticles. The ability to identify magnetic nanoparticles is extremely useful for studying complex nanoparticles assemblies comprised of magnetic and non-magnetic species.

Dipolar forces between the magnetic nanoparticles also affect the observed features in the MFM images. Puentes and co-workers have investigated the magnetic microstructure of different assemblies of cobalt nanoparticles using MFM and magnetometric measurements.<sup>183</sup> From their measurements, they have noted that when the areal density of nanoparticles is higher than certain threshold, the 2D assembly behaves like a continuous ferromagnetic thin film. The assembly is characterized by correlated areas (nearly ten particles in diameter), which are similar to domains, of parallel magnetization. Fig. 19 shows the topography and MFM image of a densely packed monolayer of Co nanoparticles (12 nm in diameter). While the topography image clearly reveals the dense packed nanoparticles, the MFM image exhibits large circular domain structures (100–300 nm wide) with alternating contrast. The lighter domains represent the areas of tip–sample repulsion while the darker regions correspond to the attractive interactions. This magnetic percolation (larger domains) was found to be mediated by dipolar interactions and the authors concluded that the magnetic microstructure, its distribution and stability strongly depends on the topological distribution of the dipoles. In the case of 3D assemblies, the magnetic microstructure was found to be less stable with the consecutive MFM images in the same locations varying with each cycle.

One of the important advantages of MFM technique (compared to Lorentz electron microscopy or spin polarized scanning tunneling microscopy) is that it can be employed to probe the magnetic microstructure of magnetic structures covered with a thin layer of non-magnetic material. Sun *et al.* have described the polymer-mediated assembly of FePt nanoparticles using PVP and PEI polymers.<sup>184</sup> The assembly process involved the exchange of oleic acid/oleyl amine around the magnetic nanoparticles with a functional polymer that is previously deposited on a substrate. Fig. 20 shows the topography and the corresponding MFM image of a three-layer 4 nm Fe<sub>58</sub>Pt<sub>42</sub> assembly treated with a pulsed laser under a perpendicular magnetic field (2.5 kOe). The AFM image shows that the smooth FePt nanoparticle assembly is intact after the laser treatment. The dark spots in MFM image indicate the magnetization pointing to the out of the particle assembly plane.

Bliznyuk and co-workers have employed MFM to probe the magnetic ordering of the self-assembled Ni nanochains discussed in Section 2.<sup>26</sup> Fig. 21a depicts the topography and Fig. 21b

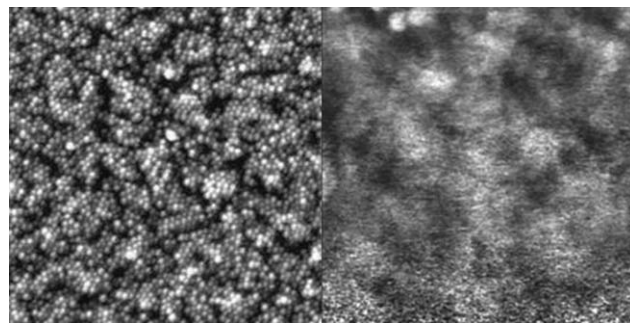


**Fig. 19** Topography (left) and MFM (right) images of 12 nm 2D assembly of cobalt nanoparticles. Z scale: (left) 10 nm and (right) 2°. Reprinted from ref. 183.



shows the corresponding MFM image on a Ni nanochain sample. While the topography image demonstrates a granular nature of the chains, the MFM image reveals variation of the dipolar magnetic stray field along the chains with the most probable arrangement of magnetic moments perpendicular to the chain line. The authors noted that in the case of head-to-tail 'ferromagnetic type' (Fig. 21c) arrangement of the magnetic moments within a nanochain, an attraction–repulsion interaction between the tip and the nanoparticles would reproduce exactly their topography image (higher interaction near nanoparticle centers and weaker interactions near inter-particle boundaries). In the case of anti-parallel antiferromagnetic type arrangement of magnetic moments along the chain of nanoparticles, more complex pattern is predicted. Because of relatively long-range forces of magnetic interactions, the AFM tip 'feels' neighboring particles (with orientation of the local magnetic field opposite to the magnetic field of the particle being probed at a given point of time). The strength of magnetic interaction between the tip and a nanoparticle is higher when the tip is located out of the center of particular particle (due to interaction with the neighboring particles) but weaker near the center and on the boundaries. This multi-particle interaction manifests itself as an appearance of a 'granular' structure (Fig. 21b), which is significantly different from AFM topography image (Fig. 21a). In the suggested model (Fig. 21c), each nanoparticle represents one small ferromagnetic domain (*i.e.* a domain with uniform orientation of the magnetic field of the magnetic moment). Therefore, the chains of Ni nanoparticles are one-dimensionally antiferromagnetically ordered. This conclusion was also supported by SQUID measurements.

## 6. Applications of self-assembled nanomagnetic systems

### 6.1 High density data storage

Applications of magnetic nanoparticles in general and self-assembled nanomagnetic systems in particular are plentiful ranging from promising medical applications to modern information technologies. The availability of ultra-high density magnetic data storage devices at low costs fuels to a large extent today's information age. The success of data storage technology is most evidently quantified in Moore's law which holds and has been originally formulated for integrated electronic circuits but is

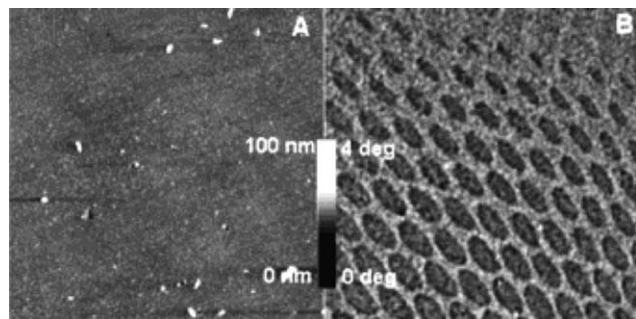


**Fig. 20** (A) AFM topography, (B) MFM image of a three-layer 4 nm  $\text{Fe}_{58}\text{-Pt}_{42}$  nanoparticle assembly annealed at 530 °C. Whereas the AFM reveals the smooth surface topography of the assembly, the MFM image reveals the assembled particles. Reprinted from ref. 184.

applicable with the same accuracy to data storage devices, most prominently for magnetic hard disk drives (HDD).<sup>185</sup>

The ever decreasing physical size of a magnetic bit in modern HDD gives rise to the fact that as long as the grain size is kept constant the number of individual magnetic grains within a magnetic bit is decreasing with increasing storage density. Grain boundaries give rise to fuzziness in the interface separating magnetic bits from each other and, hence, create noise during the read-out process. In addition to these geometrical fluctuations there can be fluctuations in the magnetic properties such as crystalline anisotropy and the corresponding orientation of the easy axis. All together such fluctuations give rise to what is known as transition jitter noise. As a consequence, the signal-to-noise ratio, which scales with the logarithm of grains per bit, becomes unfavorable when the number of grain boundaries per bit is so low that statistical averaging is no longer effective.<sup>186</sup> A possible solution is to avoid grain boundaries and statistical fluctuations within a magnetic bit all together and ultimately move to the storage of a single bit in an individual structure of well defined shape which simultaneously is magnetically single domain. Still more realistically today is the approach to reduce the grain size such that each grain with its fluctuating properties is replaced by a single domain nanoparticle with better defined shape and magnetic parameters while the magnetic bit contains a collection of identically magnetized nanoparticles. There are, however, numerous problems which accompany this approach and are understandable and addressable from the discussion of magnetic nanoparticles we made above.

A fundamental problem for magnetic data storage is the stability of the bit information when the area holding the physical information is scaled down in size. This is of particular relevance in longitudinal recording. Perpendicular media can help to overcome this problem when the reduction of the surface area of the bit is compensated for with volume gain in the depth of the film in combination with antiferromagnetic coupling schemes.<sup>187,188</sup> As outlined prior to this chapter, at temperatures above the blocking temperature the magnetization in a magnetic single domain particle starts to rotate *via* thermal activation. As a result, the time-averaged magnetization is zero and, hence, the information stored in the bit which is encoded in the magnetization orientation is lost. The blocking temperature in turn is determined by the anisotropy energy which decreases linearly with decreasing particle volume. Consequently, there is an ongoing search in materials science for optimized anisotropy constants which are high enough to ensure stability of the magnetic bit for 10 years or more at room temperature and low enough to still allow for writing of the bit.<sup>189</sup> As a rule of thumb the anisotropy energy  $KV$  of the particle must be 60 times larger than the typical thermal energy  $k_{\text{B}}T$  at room temperature to fulfill the 10 year stability criterion while the coercivity increases unfavorably with increasing anisotropy. For a single domain Stoner–Wohlfarth particle of saturation magnetization  $M_{\text{s}}$  the coercive or switching field  $H_{\text{s}}$  and the effective anisotropy  $K$  are related *via*  $H_{\text{s}} = 2K/M_{\text{s}}$ . Conflicting demands of low enough switching field and high enough anisotropy can be fulfilled simultaneously by taking advantage of the temperature dependence of coercivity and anisotropy in temperature assisted writing schemes such as the heat-assisted magnetic recording (HAMR).<sup>190</sup>



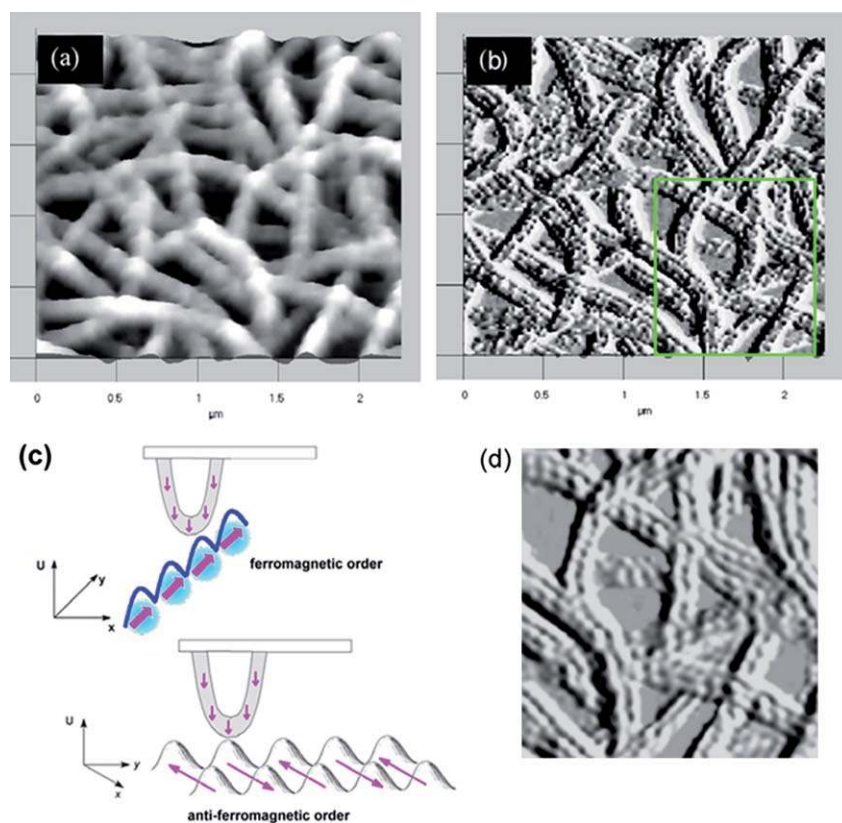


**Fig. 21** (a) AFM topography and (b) MFM images of the same region of Ni nanochains on silicon substrate. (c) Schematic of the suggested mechanism for the observed MFM contrast with antiferromagnetic order of magnetic Ni nanoparticles along the chain. Arrows show orientation of magnetic moments of individual nanoparticles and that of the AFM tip coated with Co and magnetized in the direction along the tip.  $U$  represents repulsive interaction of the AFM tip with the sample;  $y$  is direction along the chain; and  $x$  across the chain. In the case of ferromagnetic arrangement of the magnetic moments within the chain (top portion) MFM signal roughly resembles the topography while in the case of antiferromagnetic order (bottom portion) the chain appears as a two strand line of bumps due to the possible interaction of the tip with the magnetic moment of the closest nanoparticle as well as with the magnetic moments of neighboring nanoparticles. (d) Zoom-in of the MFM image followed by high frequency Fourier filtration, emphasizing the existence of magnetic field variation along the chains corresponding to antiparallel arrangement of magnetic moments as shown in portion (c). Reprinted from ref. 26.

Patterned media are a way to push the data storage density to the many TB per  $\text{in}^2$  regime.<sup>191,192</sup> A modern overview of advanced magnetic nanostructures in general and *via* self-assembly patterned nanomagnetic thin films in particular can be found in ref. 193.

Self-assembly can be considered nature's "free ride" towards a low-cost, massive parallel deposition process into well defined patterned structures rather than using expensive top-down approaches such as optical or even X-ray or e-beam lithography. The process of self-assembly allows to a certain degree to tailor fine-structured architectures of single domain size with uniform size distribution and homogeneity in their magnetic properties.<sup>194</sup> A prominent example is given by the self-assembly of FePt nanoparticles which are known for the high uniaxial anisotropy enabling thermal stability down to nanoparticle sizes of only 4 nm.<sup>195</sup> As outlined above, self-assembled magnetic nanoparticles are able to provide the necessities for ultra-high density data storage media. They have the potential to fulfill the required low noise read criteria at highest areal data density, the possibility to write with sufficiently low writing-fields while ensuring data stability for at least 10 years at low production costs, the ultimate measure for mass data storage devices.

## 6.2 Nanoelectronics and spintronics applications

Magnetic nanoparticles offer new opportunities in fabrication of nanoscaled electronic devices. One of the possible applications of metallic nanoparticles is in so-called single electron devices.<sup>196–199</sup> The devices can control the motion of a single electron or a few electrons using the principle of Coulomb blockade effect.<sup>3</sup> In a simplest device of such kind (Fig. 22) a nanosized metallic particle (island) is put into a close vicinity of two electrodes: so-called, reservoir and operating electrode (the gate). If the bias voltage created by the gate electrode is exceeding the value of  $e/C$  (where  $e$  is an electron charge and  $C$  is capacitance of the nanoparticle) it can cause tunneling an electron from the reservoir to the nanoparticle. The tunneling event will increase the charge of the nanoparticle by one electron charge, which in turn will change its energy by the value of  $E = e^2/2C$ . Therefore, the next electron will have to overcome this additional energy barrier in order to be transferred to the nanoparticle. For relatively large micrometre scale particle, the corresponding energy barrier is smaller than thermal energy at room temperature ( $k_B T = 25$  meV) and electrons can easily jump back and forth between the reservoir and the nanoparticle. However, similarly to super-

paramagnetic state, when the particle is small enough ( $\sim 10$  nm) or the temperature is low ( $\sim 1$  to 10 K) the energy barrier is significant and the next electron can be transferred only with application of a threshold voltage exceeding  $e/C$  value. Otherwise strong electrostatic repulsion (Coulomb blockade) will block the transfer of the next charge. As a result, current–voltage characteristic of the device has a characteristic staircase shape (Fig. 22b).<sup>3</sup> Single electron device can be constructed *via* self-assembly of metallic nanoparticles on patterned metallic electrodes to create a metal–organic molecule–metal junction. Single electron transistors (SETs) and many other single electron devices (pumps, turnstiles *etc.*) can be created in a similar fashion to perform various functions like electron transfer, switching or information storage.<sup>196</sup>

Even more intriguing effects and phenomena may be observed when magnetic properties of the nanoparticles are also employed.<sup>200</sup> This constitutes the subject of special spin-selective type of electronics (spintronics).<sup>201–204</sup> The giant magnetoresistance (GMR) phenomenon was the first example of the utilization of the electron spin in nanostructured electronic devices as an additional “degree of freedom”.<sup>205,206</sup> Another effect used in spintronics is tunneling magnetoresistance (TMR).<sup>207–209</sup> This effect employs a magnetic tunnel junction composed of two ferromagnetic layers separated by a thin insulating barrier.<sup>210,211</sup> TMR is used in magnetic random access memories (MRAMs) that combine the advantages of the short access time of the semiconductor RAM and the non-volatility of the magnetic memories.<sup>212</sup>

In a last decade significant interest has been attracted by semiconductor spintronics which utilizes semiconducting materials to inject, detect and transport electron’s spins.<sup>213</sup> In particular, conventional semiconductors, such as GaAs and CdTe, doped with transition metal magnetic atoms like Mn, have been intensively studied.<sup>214,215</sup> The challenge is to find a dilute magnetic semiconductor that has the Curie temperature above the room temperature.<sup>216</sup> The prospect of semiconductor spintronics offers an intriguing possibility to combine well-established semiconductor technology with novel spin-related functionalities.<sup>217,218</sup> More recently a new direction in spintronics has emerged, which involves hybrid structures involving magnetoelectric, ferroelectric and multiferroic materials.<sup>219–221</sup>

Spintronics exploits the spin of an electron to process or store digital information. For example, one of the simplest spintronics

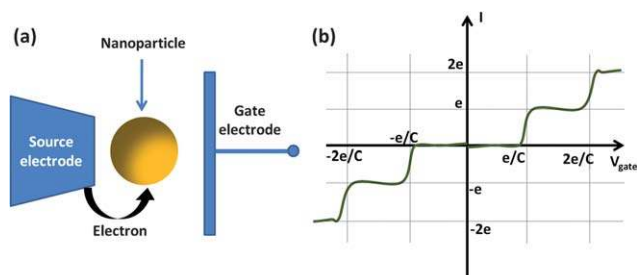


**Fig. 22** (a) Simple single electron transistor structure employing a metallic nanoparticle assembled between the source and gate electrodes; (b) typical Coulomb staircase current–voltage characteristic of a SET. Current ( $I$ ) is proportional to the variation of the charge ( $\Delta Q$ ) under applied bias voltage and is quantized with the electron charge  $e$ .

devices is a spin valve exhibiting a GMR effect. GMR is the large change in electrical resistance of metallic layered systems when the magnetizations of the ferromagnetic layers are reoriented relative to one another under the application of an external magnetic field.<sup>222</sup> As shown in Fig. 23, the resistance of the spin valve is different depending on whether the orientation of magnetic moments in two magnetic layers separated with a nonmagnetic metallic layer is parallel or antiparallel. The relative difference in resistance between parallel and antiparallel magnetizations, known as the GMR ratio, can reach 200% for some structures.

A similar effect is observed when magnetic nanoparticles are embedded in a non-magnetic metallic matrix. When a ferromagnetic metal is alloyed with a non-magnetic metal, it precipitates into granules, as is schematically shown in Fig. 24 (top). The size of the granules depends on the solubility of the ferromagnetic material in the nonmagnetic matrix and on growth and annealing conditions and can be as small as 2 nm. In the absence of the applied field their magnetic moments are randomly oriented. Applying a magnetic field aligns the moments of the granules, which results in the resistance drop due to a GMR effect. This behavior is illustrated in Fig. 24 (bottom), which displays the field dependence of the relative change in the resistance for heterogeneous  $\text{Co}_x\text{Cu}_{1-x}$  alloys.<sup>223</sup> This earlier demonstration of GMR in granular materials was followed by numerous more recent investigations. Unfortunately, the saturation fields, which are required to align the moments, are relatively high (of the order of 10 kG) which makes the applicability of granular materials fairly limited. In addition, the magnitude of GMR at room temperature is strongly reduced due to superparamagnetic relaxation, which originates from thermal fluctuations of the magnetic moments of the granules.

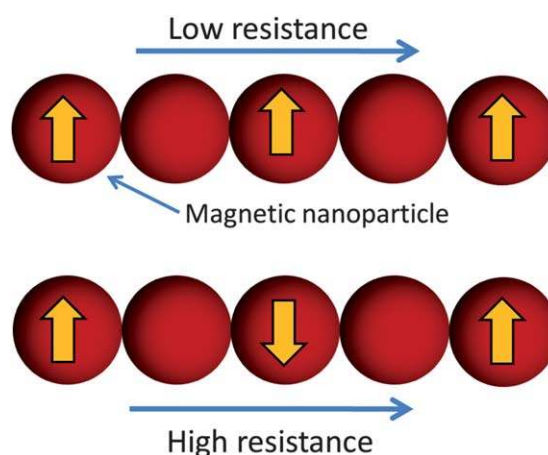


**Fig. 23** Hypothetic self-assembled nanostructured devices with (bottom) high-resistance and (top) low-resistance geometry of charge polarization GMR (if the spacer particles shown with a filled sphere is a nonmagnetic metal) or TMR effect (if the spacer particles are insulators). Arrows indicate the magnetization direction of the superparamagnetic nanoparticles. For applications, magnetic moment of one of the particles has to be “pinned” through the shape anisotropy and may be exchange-biased while the other magnetic dipoles are reoriented by the external magnetic field. The spacer nanoparticle can be replaced by a shell layer in core–shell system approach.

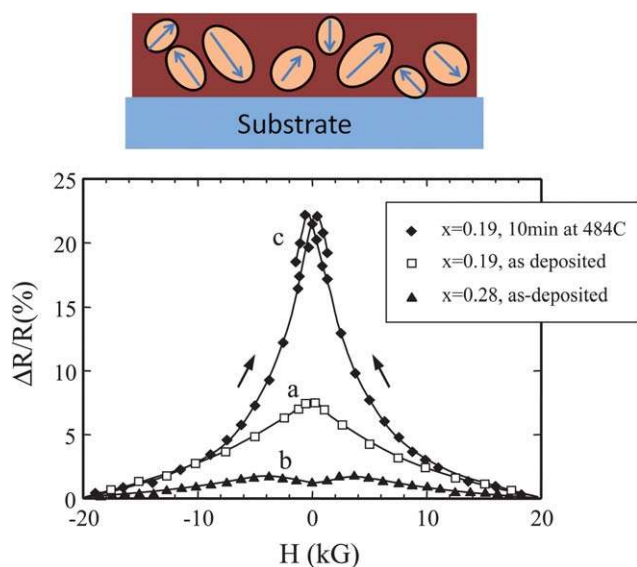


**Fig. 24** (Top) Magnetic nanoparticles embedded in a non-magnetic metallic or insulating material deposited as a thin film on a substrate. In the absence of the field the magnetic moments of the nanoparticles are randomly oriented. Magnetic field aligns the moments and leads to a resistance change in the system, manifesting the GMR effect in the case of metallic matrix and the TMR effect in the case of insulating matrix. (Bottom) Magnetic field dependence of  $\Delta R/R = [R(H) - R(H = 20 \text{ kG})]/R(H = 20 \text{ kG})$  in granular  $\text{Co}_x\text{Cu}_{1-x}$  films. Curves *a* and *b* measured at  $T = 100 \text{ K}$ , curve *c* measured at  $T = 10 \text{ K}$ . Reprinted from ref. 223.

In magnetic tunnel junctions two ferromagnetic layers (or nanoparticles) are separated by a thin insulating barrier. The first particle serves to polarize the spins of electrons which are crossing the barrier by quantum mechanical tunneling before reaching the second particle (or ferromagnetic layer). Two magnetic particles are aligned to have either parallel or antiparallel orientation of magnetic layers. When their magnetic moments are parallel electrons can pass the device's junction easier in comparison to the antiparallel orientation of magnetizations when the tunneling is significantly reduced due to the TMR effect.<sup>210</sup> The magnitude of the current can be used therefore to define two states and to indicate digital "1" and "0" in a magnetic random access memory (MRAM) device. Considering a nanometre size of the nanoparticles this may create a route for high density data storage employing a TMR effect.

The TMR effect can also be observed in granular solids composed of nanometre-size ferromagnetic particles in an insulating matrix (see Fig. 24, top).<sup>224–226</sup> Similar to GMR counterparts, these materials have lower resistance when all magnetic particle moments are aligned by an applied magnetic field than in the case of randomly orientated moments. It was predicted that TMR in these materials is weakly temperature dependent due to the charging energy  $E_c$  that adds a factor of  $\exp(-E_c/kT)$  in the expression for conductance.<sup>227</sup> This prediction is confirmed experimentally for Co nanoparticles in  $\text{ZrO}_2$  insulating thin films.<sup>228</sup> The weak temperature dependence of the magnetoresistance makes granular materials with insulating matrices more attractive from the point of view of applications, as compared to those with metallic matrices.

As predicted by theory,<sup>229–232</sup> spin-dependent tunneling in combination with the Coulomb blockade regime can lead to both an enhancement and an oscillatory bias dependence of the TMR. Realizing a system where these effects can be observed, however, is an experimental challenge. Granular systems, such as Co clusters in  $\text{Al}_2\text{O}_3$  are by far the easiest, and an enhancement of the TMR at low temperatures has been demonstrated,<sup>233,234</sup> but the wide distribution of cluster sizes, and hence charging energies, tends to smear out the predicted oscillatory behavior of the TMR. This problem was addressed by depositing a granular film in a nano-scale constriction, such that the number of clusters within the measured region is small (see Fig. 25a). By additionally gaining better control over the size distribution of the clusters, the predicted oscillatory behavior of the TMR was demonstrated (see Fig. 25b and c).<sup>235,236</sup>

In addition to standard magnetic materials, such as Fe, Co, Ni or their alloys, spintronics can employ special materials which exhibit high (nearly 100%) level of spin polarization. Heusler alloys with the general composition  $\text{X}_2\text{YZ}$  where X may be for example Co or Fe, Y may be Mn and Z may be Al or Si or  $\text{CrO}_2$  are considered to be prominent for such applications.<sup>204</sup> The effect is due to a finite density of states at the Fermi level for one spin direction and appearance of an energy gap for the other spin direction, as a consequence of the hybridization of metal d-states on X and Y constituents.

One more type of nanoparticles which can be employed in this field is a class of some magnetically doped oxide semiconductors. The nature of ferromagnetism in such systems (Co, Fe, or Cr doped ZnO,  $\text{TiO}_2$  or other materials) is still debated and the reports range from no ferromagnetic properties at room temperature<sup>237</sup> to intrinsic and strong ferromagnetism at room temperature and above.<sup>238</sup>

A prospective type of spintronic materials is a combination of magnetic nanoparticles with a semiconducting organic (or polymer) matrix (polyaniline or polythiophenes type conjugated polymers can be employed). Such hybrid materials can in principle combine the best characteristics of the matrix (mechanical flexibility, optical transparency, semiconducting properties, etc.) with magnetic interactions between imbedded magnetic moments. Moreover, as demonstrated in ref. 239 formation of regular arrays of nanoparticles (Co) is possible due to their polymer-assisted self-assembly in polyaniline matrix. Development of polymer based spintronic materials is still in infancy.

### 6.3 Biomedical applications

Magnetic nanoparticles are being extensively investigated for various biomedical applications, which include targeted drug delivery as magnetic vectors can be directed to the target of interest using either external or internal magnetic field, magnetic contrast agents in magnetic resonance imaging (MRI), hyperthermia agents for localized damage of the tumor tissue using high frequency magnetic field, and cell and biomolecule separation. While the reports so far primarily involve tailoring individual magnetic nanostructures (size, shape and surface chemistry), collective physical properties of magnetic nanostructure assemblies are promising for future biomedical applications.



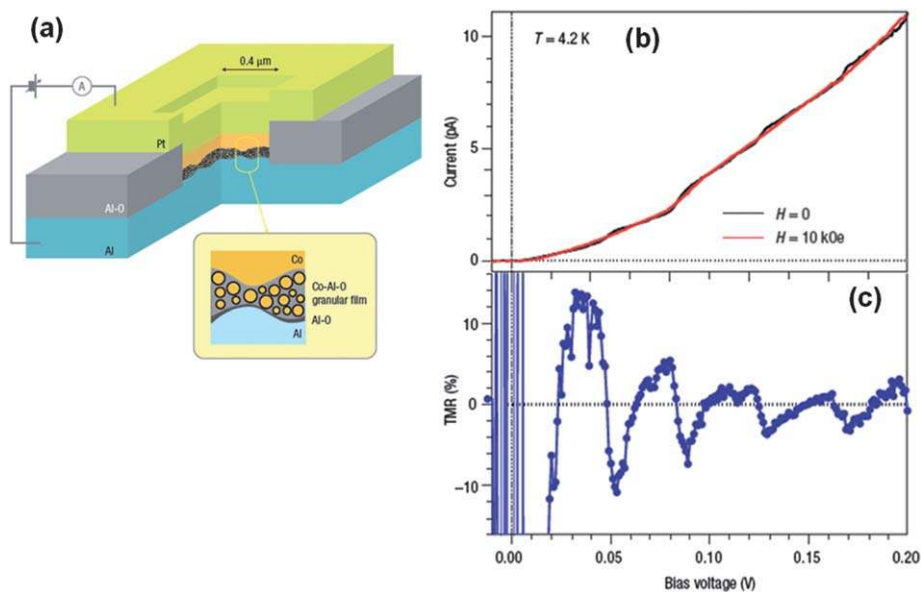


**Fig. 25** (a) Schematic structure of a pillared architecture device prepared for current measurements. The bottom Al electrode is coated with Al-O and Co-Al-O granular film, then with Co top electrode and with Pt layer microfabricated by electron-beam lithography and Ar-ion milling process to reduce the contact area to a sub-micrometre scale. The nominal thickness of the active Co-Al-O layer is 15 nm (which corresponds to only 3 to 4 particles), but current-dominating path has only one or two particles involved due to the electrodes roughness as shown in the inset. (b) Corresponding current-bias curves measured at 4.2 K and (c) bias dependence of the tunnel magnetoresistance (TMR). In (b) the black and the red curves represent a clear Coulomb staircase dependence at zero magnetic field and applied field of 10 kOe, respectively. TMR behavior in (c) demonstrates oscillation with alternate sign change. Reprinted from ref. 235.

**6.3.1 Drug delivery.** Drug delivery, involves targeted delivery of payload to the vicinity of the target, typically tumor site. Numerous material systems such as micelles, plasmonic nanostructures, liposomes, layer by layer assembled polymer capsules, dendrimers have been investigated for drug delivery applications. Magnetic nanostructures offer certain unique advantages compared to most of these systems such as (i) they can be guided to the target site using external (or internal) magnetic field, (ii) triggered release of the external drug by heating the magnetic nanostructures using magnetic field and (iii) they can be visualized in the body using magnetic resonance imaging.

One of the important aspects that need to be considered in the context of using magnetic nanostructures for drug delivery applications (or more generally for biomedical applications) is the surface modification of the nanostructures.<sup>240</sup> Although nanostructures without specific targeting agents on the surface (also called passive targeting), which rely on enhanced permeation and retention (EPR) effects (owing to the leaky blood vessels of tumor sites) have been employed for various biomedical applications, they typically exhibit poor results. Typical chemical synthesis of magnetic nanostructures results in hydrophobic hydrocarbons. For enhancing the biocompatibility and achieving specific targeting capability the magnetic nanostructures, surface modification can be achieved by adding amphiphilic surfactants or through ligand exchange reactions. The hydrophobic part of the amphiphilic molecule interacts with the existing hydrocarbon chain on the magnetic nanostructure while the hydrophilic makes the nanoparticles water soluble and biocompatible. On the other hand, ligand exchange reactions involve in the displacement of the existing ligands and replacement with a bifunctional ligand with one functional group

strongly interacting with the nanoparticle while the other functional group renders other desired functionality (e.g. water solubility, reduce leaching, avoiding reticuloendothelial system (RES) clearance thus improving the half-life in the blood stream).

Numerous (bio)polymers, organic molecules and inorganic coatings have been employed in the surface modification of the magnetic nanostructures such as poly(ethylene glycol), poly(vinyl pyrrolidone), poly(ethylene-co-vinyl acetate), poly(vinyl alcohol), dendrimers, silanes, proteins and silica.<sup>241–247</sup> A variety of drugs such as cisplatin,<sup>248,249</sup> methorexate,<sup>250</sup> mitoxantrone,<sup>251,252</sup> tamoxifen,<sup>253</sup> danorubicin,<sup>254</sup> doxorubicin<sup>255</sup> and fludarabine<sup>256</sup> have been loaded into the porous organic or inorganic shells of the surface-modified magnetic nanoparticles. Some of the general issues or challenges associated with the deployment of magnetic nanoparticles for drug delivery (or gene delivery) applications include (i) improving biocompatibility or obtain control over *in vivo* behavior, (ii) achieving control over bioelimination (which includes preventing unwanted clearance and enabling safe clearance when desired), (iii) improving specific targeting, (iv) minimizing the polydispersity (of size, surface functionality) and (v) issues related to the limited penetration of the magnetic field deep into the body.

**6.3.2 MRI contrast agents.** Superparamagnetic nanoparticles are being extensively investigated as contrast agents in magnetic resonance imaging (MRI).<sup>257,258</sup> In the presence of an external magnetic field the superparamagnetic nanoparticles shorten the spin-spin relaxation time ( $T_2$ ) of the water protons around them, resulting in darkening of these regions in the  $T_2$  weighted images.

Metals alloys and metal oxide magnetic nanostructures have been employed as magnetic contrast agents in MRI imaging. For effective deployment as contrast agents, one has to ensure specific targeting of the magnetic nanoparticles to the desired tissues. Again the same set of problems discussed in the case of drug delivery hamper the application of magnetic nanostructures as contrast agents. Unwanted elimination of magnetic nanostructures by RES clearance processes and their non-specific accumulation in liver, spleen, lymph nodes clearly pose significant challenges. Specific targeting of the nanoparticles involves in the surface functionalization of the nanoparticles with different kinds of targeting agents.

Iron oxide nanoparticles with and without specific targeting have been employed as contrast agents. Cheon and coworkers synthesized herceptin-conjugated iron oxide nanoparticles, which can selectively bind to the epidermal-growth factor receptor (Her2/neu), which is usually overexpressed in breast cancers.<sup>259</sup> This active targeting enabled them to image the tumor cells selectively. Numerous other actively targeted nanostructures such as anti-carcinoembryonic antigen conjugated iron oxide nanoparticles, chlorotoxin conjugated PEG-coated iron oxide particles have been employed for enhancing contrast in magnetic imaging.<sup>260,261</sup>

Lee and coworkers have demonstrated the use of magnetic nanoparticles with high magnetization, which exhibited more sensitive *in vivo* MR targeted imaging.<sup>262</sup> The authors investigated a series of metal-doped magnetism engineered iron oxide nanoparticles of spinel  $MFe_2O_4$  where M is +2 cation of Mn, Fe, Co or Ni. Herceptin conjugated manganese doped magnetism engineered iron oxide (MnMEIO) nanoparticles exhibited highly sensitive targeted *in vivo* mice imaging. In fact the particles exhibited sufficient sensitivity to image even very small tumors on mice. Fig. 26 shows the MR images obtained at various times after the injection of herceptin conjugated MnMEIO and crosslinked iron oxide (CLIO). It can be clearly seen from the color changes that the contrast in the case of MnMEIO (color change from red to blue) increases with time due to the progressive targeting while no change was observed in the case of CLIO. They clearly demonstrated that high-magnetic moment nanoparticles and appropriate targeting agents are capable of providing a powerful platform for ultrasensitive detection of various types of cancer.

Even more recently, there have been various reports of multifunctional nanoparticles comprised of various metals (*e.g.* magnetic ( $Fe_3O_4$ , Fe–Pt) and plasmonic (Au, Ag) optical (quantum dots)), which can impart multifunctionality.<sup>263</sup> For example, dumb-bell like nanostructures comprised of magnetic and plasmonic nanoparticles were employed for magnetic and optical imaging.<sup>264</sup> Similar approaches have been employed for achieving nanostructures, which can serve the dual purpose of imaging and therapy. The readers are referred to a recent review on the subject for comprehensive discussion.<sup>265</sup> Multifunctionality which is achieved by structural integration of multiple nanocomponents will remain an active research area owing to the potential applications of such nanostructures in various biomedical applications.

**6.3.3. Hyperthermia using magnetic nanoparticles.** Another important application of magnetic nanostructures that is being

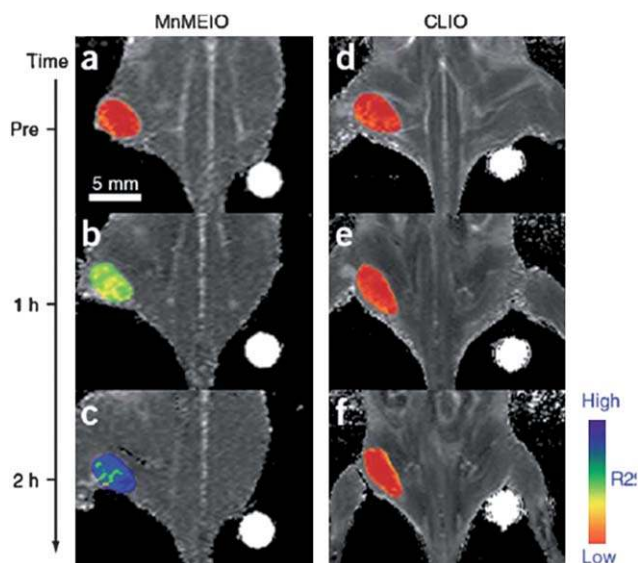


**Fig. 26** Color coded MR images obtained at various times after the injection of herceptin conjugated MnMEIO and crosslinked iron oxide (CLIO). The images show that the contrast in the case of MnMEIO (color change from red to blue) increases with time due to the progressive targeting while no change was observed in the case of CLIO. Reprinted from ref. 262.

widely investigated is hyperthermia using nanomagnetic structures. This approach of cancer therapy does not involve any drugs for treating cancer. Instead, the magnetic nanostructures under external magnetic field cause local heat, which results in suppression of the cancer cells. The technique, often referred to magnetic hyperthermia, is an important therapeutic technique that is being extensively investigated with a wide variety of magnetic nanostructures. The local heating can result from both hysteresis and relaxation losses.<sup>266,267</sup> In the case of ferromagnetic nanostructures, the hysteresis loss contributes to the magnetic hyperthermia while in the case of superparamagnetic nanostructures relaxation losses play a major role. The general strategy of magnetic hyperthermia involves surface functionalization of magnetic nanostructures with targeting agents to selectively accumulate at the tumor site followed by subjecting the nanostructure to external AC magnetic field, which rises the local temperature to above 40 °C, resulting in tumor suppression.<sup>268,269</sup> The field remains extremely active with novel multifunctional nanostructures and surface functionalization strategies and *in vivo* studies being the mainstay.<sup>270</sup>

## 7. Conclusions and outlook

Large scale assembly of nanomaterials into well-defined superstructures is an important pre-requisite for attaining ultimate control over their properties and to realize (multi-) functional systems and sub-systems based on these nanostructures. Self-assembly of nanostructures is believed to be a powerful tool to address the aforementioned challenge. In contrast to non-magnetic nanostructures, magnetic nanostructures offer a facile handle in the form of “response to magnetic field” to enable complex superstructures. The dipolar forces of magnetic nanostructures are directional in nature, providing facile control over

self-assembly and enabling richer morphologies such as close-packed monolayers, 3D crystals, chains, rings, and loops. This review provides a snapshot of recent progress in magnetic nanoparticles where we have briefly introduced the most important chemical and physical methods for the synthesis of magnetic nanoparticles, their size dependent properties and applications. Numerous self- and directed assembly strategies, which have been introduced over last decade, have been highlighted. Important characterization techniques such as SQUID magnetometry and magnetic force microscopy, which provide deeper insight into the collective magnetic properties of the assembled structures have been discussed with particular emphasis to recent findings related to the interpretation of the experimental results. Self-assembled magnetic nanostructures are expected to find important applications in high density information storage with extremely high areal density, spintronic devices and various biomedical applications.

While there has been significant progress in the size and shape controlled synthesis of magnetic nanostructures and their assembly, there are several challenges that need to be addressed before we can tap into the full potential of magnetic nanostructures. The shape controlled synthesis of magnetic nanostructures lags behind that achieved in the case of plasmonic nanostructures such as gold and silver nanostructures, where different complex shapes such as “nano-rice”, “nano-crescents”, and “nano-stars” are routinely fabricated.<sup>271,272</sup> A fine adjustment of the shape of the nanostructures would allow better control over their properties and their assembly. The self-assembly methods demonstrated so far are primarily limited to fabrication of rather simple structures such as linear arrays, rings, close packed structures and typically involve non-specific interactions. A higher degree of control and large scale uniformity are critical for realizing self-assembled high density storage devices, spintronic devices and magnetic sensing devices. Yet another exciting direction, which is in its infancy is dynamic or responsive magnetic assemblies, which can be reversibly reconfigured using external stimuli such as pH, temperature, and light. Generally, such “smart” nano-materials offer great promise in achieving adaptive materials whose properties can be reversibly tuned or altered upon demand.

## References

- 1 A. C. Edrington, A. M. Urbas, P. DeRege, C. X. Chen, T. M. Swager, N. Hadjichristidis, M. Xenidou, L. J. Fetters, J. D. Joannopoulos, Y. Fink and E. L. Thomas, *Adv. Mater.*, 2001, **13**, 421.
- 2 M. Brust and C. J. Kiely, *Colloids Surf., A*, 2002, **202**, 175.
- 3 C. Petty, *Molecular Electronics from Principles to Practice*, Wiley, 2007.
- 4 D. L. Feldheim and C. D. Keating, *Chem. Soc. Rev.*, 1998, **27**, 1.
- 5 S. Kim, *Electron. Mater. Lett.*, 2007, **3**, 109.
- 6 O. A. Aktsipetrov, *Colloids Surf., A*, 2002, **202**, 165.
- 7 X. M. Lin and A. C. S. Samia, *J. Magn. Magn. Mater.*, 2006, **305**, 100.
- 8 Q. Dai and A. Nelson, *Chem. Soc. Rev.*, 2010, **39**, 4057.
- 9 K. M. Krishnan, A. B. Pakhomov, Y. Bao, P. Blomqvist, Y. Chun, M. Gonzales, K. Griffin, X. Ji and B. K. Roberts, *J. Mater. Sci.*, 2006, **41**, 793.
- 10 G. Ranjan and I. K. Puri, *Adv. Appl. Mech.*, 2006, **41**, 293.
- 11 J.-P. Wang, *Proc. IEEE*, 2008, **96**, 1847.
- 12 J. R. Choi, S. J. Oh, H. Ju and J. Cheon, *Nano Lett.*, 2005, **5**, 2179.
- 13 T. K. McNab, R. A. Fox and A. J. F. Boyle, *J. Appl. Phys.*, 1968, **39**, 5703.
- 14 Q. Chen and Z. J. Zhang, *Appl. Phys. Lett.*, 1998, **73**, 3156.
- 15 B. M. Berkovsky, Some Aspects of Theoretical Modeling of Thermomechanics of Magnetic Fluids, in *Proc. International Advanced Course and Workshop on Thermomechanics of Magnetic Fluids*, ed. B. M. Berkovsky, Hemisphere, Washington, DC, 1978, vol. 149.
- 16 K. Abe, Y. Miyamoto and S. Chikazumi, *J. Phys. Soc. Jpn.*, 1976, **41**, 1894.
- 17 *Magnetic Nanostructures*, ed. H. S. Nalwa, American Scientific Publishers, 2002.
- 18 S. L. Biswal and A. P. Gast, *Phys. Rev. E: Stat., Nonlinear, Soft Matter Phys.*, 2004, **69**, 041406.
- 19 Y. W. Jun, J. W. Seo and A. Cheon, *Acc. Chem. Res.*, 2008, **41**, 179.
- 20 M. P. Morales, S. Veintemillas-Verdaguer, M. I. Montero, C. J. Serna, A. Roig, L. Casas, B. Martinez and F. Sandiumenge, *Chem. Mater.*, 1999, **11**, 3058.
- 21 S. Linderoth, P. V. Hendriksen, F. Bodker, S. Wells, K. Davies, S. W. Charles and S. Morup, *J. Appl. Phys.*, 1994, **75**, 6583.
- 22 G. K. Kouassi, J. Irudayaraj and G. McCarty, *BioMagn. Res. Technol.*, 2005, **3**, 1.
- 23 J. Park, E. Lee, N. M. Hwang, M. S. Kang, S. C. Kim, Y. Hwang, J. G. Park, H. J. Noh, J. Y. Kini, J. H. Park and T. Hyeon, *Angew. Chem., Int. Ed.*, 2005, **44**, 2872.
- 24 V. Skumryev, S. Stoyanov, Y. Zhang, G. Hadjipanayis, D. Givord and J. Nogués, *Nature*, 2003, **423**, 850–853.
- 25 J. Eisenmenger and I. K. Schuller, *Nat. Mater.*, 2003, **2**, 437.
- 26 V. N. Bliznyuk, S. Singamaneni, S. Sahoo, S. Polisetty, S. He and C. Binek, *Nanotechnology*, 2009, **20**, 105606.
- 27 K. J. Bishop, C. E. Wilmer, S. Soh and B. A. Grzybowski, *Small*, 2009, **5**, 1600.
- 28 A.-H. Lu, E. L. Salabas and F. Schuth, *Angew. Chem., Int. Ed.*, 2007, **46**, 1222.
- 29 J. Park, K. An, Y. Hwang, J.-G. Park, H.-J. Noh, J.-Y. Kim, J.-H. Park, N.-M. Hwang and T. Hyeon, *Nat. Mater.*, 2004, **3**, 891.
- 30 S. Sun, H. Zeng, D. B. Robinson, S. Sahoo, P. M. Rice, S. X. Wang and G. Li, *J. Am. Chem. Soc.*, 2004, **126**, 273.
- 31 F. X. Redl, C. T. Black, G. C. Papaefthymiou, R. L. Sandstrom, M. Yin, H. Zeng, C. B. Murray and S. P. O'Brien, *J. Am. Chem. Soc.*, 2004, **126**, 14583.
- 32 M. Byun, J. Wang and Z. Lin, *J. Phys.: Condens. Matter*, 2009, **21**, 264014.
- 33 N. R. Jana, Y. Chen and X. Peng, *Chem. Mater.*, 2004, **16**, 3931.
- 34 G. Salazar-Alvarez, J. Qin, V. Sepelak, I. Bergmann, M. Vasilakaki, K. N. Trohidou, J. D. Ardisson, W. A. A. Macedo, M. Mikhaylova, M. Muhammed, M. D. Bar, J. Nogués and G. Salazar-Alvarez, *J. Am. Chem. Soc.*, 2008, **130**, 13234.
- 35 S. Disch, E. Wetterkog, R. P. Hermann, G. Salazar-Alvarez, P. Busch, T. Bruckel, L. Bergstrom and S. Kamali, *Nano Lett.*, 2011, **11**, 3048.
- 36 S. Sun, C. B. Murray and H. Doyle, in *Advanced Hard and Soft Magnetic Materials*, ed. M. Coey, L. H. Lewis, B.-M. Ma, T. Schrefl, L. Schultz, J. Fidler, V. G. Harris, R. Hasegawa, A. Inoue and M. McHenry, *Mater. Res. Soc. Symp. Proc.*, 1999, 577, 385.
- 37 V. F. Puentes, K. M. Krishnan and A. P. Alivisatos, *Science*, 2001, **291**, 2115.
- 38 C. B. Murray, C. R. Kagan and M. G. Bawendi, *Science*, 1995, **270**, 1335.
- 39 C. B. Murray, S. Sun, H. Doyle and T. Betley, *MRS Bull.*, 2001, **26**, 985.
- 40 F. Dumestre, B. Chaudret, C. Amiens, M.-C. Fromen, M.-J. Casanove, M. Respaud and P. Zurcher, *Angew. Chem., Int. Ed.*, 2002, **41**, 4286.
- 41 F. Dumestre, B. Chaudret, C. Amiens, M. Respaud, P. Fejes, P. Renaud and P. Zurcher, *Angew. Chem., Int. Ed.*, 2003, **42**, 5213.
- 42 N. Cordente, M. Respaud, F. Senocq, J. M-Casanove, C. Amiens and B. Chaudret, *Nano Lett.*, 2001, **1**, 565.
- 43 X. Wang, J. Zhuang, Q. Peng and Y. Li, *Nature*, 2005, **437**, 121.
- 44 S. Singamaneni and V. N. Bliznyuk, *Appl. Phys. Lett.*, 2005, **87**, 162511.
- 45 G. A. Ozin, *Adv. Mater.*, 1992, **4**, 612.
- 46 A. Huczko, *Appl. Phys. A: Mater. Sci. Process.*, 2000, **70**, 365.
- 47 C. R. Martin, *Chem. Mater.*, 1996, **8**, 1739.



- 48 S. Shingubara, *J. Nanopart. Res.*, 2003, **5**, 17.
- 49 K. Nielsch, R. B. Wehrspohn, J. Barthel, J. Kirschner, U. Gosele, S. F. Fischer and H. Kronmüller, *Appl. Phys. Lett.*, 2001, **79**, 1360.
- 50 A. J. Yin, J. Li, W. Jian, A. J. Bennett, J. M. Xu and W. Jian, *Appl. Phys. Lett.*, 2001, **79**, 1039.
- 51 J. Bao, C. Tie, Z. Xu, Q. Zhou, D. Shen and Q. Ma, *Adv. Mater.*, 2001, **13**, 1631.
- 52 S. J. Hurst, E. K. Payne, L. Qin and C. A. Mirkin, *Angew. Chem., Int. Ed.*, 2006, **45**, 2672.
- 53 M. A. Bangar, C. M. Hangarter, B. Yoo, Y. Rheem, W. Chen, A. Mulchandani and N. V. Myung, *Electroanalysis*, 2009, **21**, 61.
- 54 M. P. Zach, K. H. Ng and R. M. Penner, *Science*, 2000, **290**, 2120.
- 55 M. P. Zach, K. Inazu, J. C. Hemminger and R. M. Penner, *Chem. Mater.*, 2002, **14**, 3206.
- 56 R. M. Penner, *J. Phys. Chem. B*, 2002, **106**, 3339.
- 57 M. Z. Atashbar, D. Banerji, S. Singamaneni and V. N. Bliznyuk, *Nanotechnology*, 2004, **15**, 374.
- 58 M. Z. Atashbar, D. Banerji and S. Singamaneni, *IEEE Sens. J.*, 2005, **5**, 792.
- 59 E. C. Walter, B. J. Murray, F. Favier, G. Kaltenpoth, M. Grunze and R. M. Penner, *J. Phys. Chem. B*, 2002, **106**, 11407.
- 60 F. C. Meldrum, V. J. Wade, D. L. Nimmo, B. R. Heywood and S. Mann, *Nature*, 1991, **349**, 684.
- 61 P. Mackle, J. M. Charnock, C. D. Garner, F. C. Meldrum and S. Mann, *J. Am. Chem. Soc.*, 1993, **115**, 8471.
- 62 F. C. Meldrum, T. Douglas, S. Levi, P. Arosio and S. Mann, *J. Inorg. Biochem.*, 1995, **58**, 59.
- 63 K. K. W. Wong, T. Douglas, S. Gider, D. D. Awschalom and S. Mann, *Chem. Mater.*, 1998, **10**, 279.
- 64 O. Kasyutich, A. Sarua and W. Schwarzacher, *J. Phys. D: Appl. Phys.*, 2008, **41**, 134022.
- 65 A. Ulman, *An Introduction to Organic Thin Films*, Academic Press, San Diego, CA 1991.
- 66 J. S. Lindsey, *New J. Chem.*, 1991, **15**, 153.
- 67 V. V. Tsukruk, *Prog. Polym. Sci.*, 1997, **22**, 247.
- 68 X. C. Zhuang, C. Yu, L. Ying, C. Lianzhen, L. Ying and Y. Liu, *Progr. Chem.*, 2007, **19**, 1653.
- 69 J. P. Comrie, *Molecular Self-assembly: Advances in Chemistry, Biology and Nanotechnology*, Nova Science Publishers Inc., 2011.
- 70 R. J. Iler, *J. Colloid Interface Sci.*, 1996, **21**, 569.
- 71 B. A. Grzybowski, C. E. Wilmer, J. Kim, K. P. Browne and K. J. M. Bishop, *Soft Matter*, 2009, **5**, 1110.
- 72 Z. Nie, A. Petukhova and E. Kumacheva, *Nat. Nanotechnol.*, 2010, **5**, 15.
- 73 S. Kinge, M. Crego-Calama and D. N. Reinhoudt, *ChemPhysChem*, 2008, **9**, 20.
- 74 K. C. Barick and D. Bahadur, *J. Nanosci. Nanotechnol.*, 2010, **10**, 668.
- 75 N. V. Dziomkina and G. J. Vancso, *Soft Matter*, 2005, **1**, 265.
- 76 M. Grzelczak, J. Vermant, E. M. Furst and L. M. Liz-Marzan, *ACS Nano*, 2010, **4**, 3591.
- 77 J. N. Israelachvili, *Intermolecular and Surface Forces*, Elsevier, 3rd edn, 2011.
- 78 P. C. Scholten and D. L. A. Tjaden, *J. Colloid Interface Sci.*, 1980, **73**, 254.
- 79 Y. Lalatonne, J. Richardi and M. P. Pileni, *Nat. Mater.*, 2004, **3**, 121.
- 80 A. P. Hynninen and M. Dijkstra, *Phys. Rev. Lett.*, 2005, **94**, 138303.
- 81 D. J. Klingenberg, *AIChE J.*, 2001, **47**, 246.
- 82 J. R. Thomas, *J. Appl. Phys.*, 1966, **37**, 2914.
- 83 M. Tanase, L. A. Bauer, A. Hultgren, D. M. Silevitch, L. Sun, D. H. Reich, P. C. Searson and G. J. Meyer, *Nano Lett.*, 2001, **1**, 155.
- 84 H. L. Niu, Q. W. Chen, H. F. Zhu, Y. S. Lin and X. Zhang, *J. Mater. Chem.*, 2003, **13**, 1803.
- 85 M. Tanase, D. M. Silevitch, A. Hultgren, L. A. Bauer, P. C. Searson, G. J. Meyer and D. H. Reich, *J. Appl. Phys.*, 2001, **91**, 8549.
- 86 S. L. Tripp, S. V. Pusztyai, A. E. Ribbe and A. Wei, *J. Am. Chem. Soc.*, 2002, **124**, 7914.
- 87 S. L. Tripp, R. E. Dunin-Borkowski and A. Wei, *Angew. Chem., Int. Ed.*, 2003, **42**, 5591.
- 88 K. Butter, P. H. H. Bomans, P. M. Frederik, G. J. Vroege and A. P. Philipse, *Nat. Mater.*, 2003, **2**, 88.
- 89 A. Goyal, C. K. Hall and O. D. Velev, *Phys. Rev. E: Stat., Nonlinear, Soft Matter Phys.*, 2008, **77**, 031401.
- 90 T. Tlusty and S. A. Safran, *Science*, 2000, **290**, 1328.
- 91 L. Zhou, W. J. Wen and P. Sheng, *Phys. Rev. Lett.*, 1998, **81**, 1509.
- 92 G. Cheng, D. Romero, G. T. Fraser and A. R. Hight Walker, *Langmuir*, 2005, **21**(26), 12055–12059.
- 93 W. L. Zhou, E. E. Carpenter, J. Lin, A. Kumbhar, J. Sims and C. J. O'Connor, *Eur. Phys. J. D*, 2001, **16**, 289.
- 94 J. Li, Q. Ye, A. Cassell, H. T. Ng, R. Stevens, J. Han and M. Meyyappan, *Appl. Phys. Lett.*, 2003, **82**, 2491.
- 95 M. P. Pileni, *J. Phys. Chem. B*, 2001, **105**, 3358.
- 96 T. M. Whitney, J. S. Jiang, P. C. Searson and C. L. Chien, *Science*, 1993, **261**, 1316.
- 97 J. Bansmann, S. H. Baker, C. Binns, J. A. Blackman, J.-P. Bucher, J. Dorantes-Davila, V. Dupuis, L. Favre, D. Kechrakos, A. Kleibert, K.-H. Meiwes-Broer, G. M. Pastor, A. Perez, O. Toulemonde, K. N. Trohidou, J. Tuaille and Y. Xie, *Surf. Sci. Rep.*, 2005, **56**, 189.
- 98 C. Raj Sankar, S. Vijayanand, S. Verma and P. A. Joy, *Solid State Commun.*, 2007, **141**, 307.
- 99 J. L. Kirschvink, M. M. Walker and C. E. Diebel, *Curr. Opin. Neurobiol.*, 2001, **11**, 462.
- 100 C. M. Liu, L. Guo, R. M. Wang, Y. Deng, H. B. Xu and S. Yang, *Chem. Commun.*, 2004, 2726.
- 101 H. Wang, Q. W. Chen, L. X. Sun, H. P. Qi, X. Yang, S. Zhou and J. Xiong, *Langmuir*, 2009, **25**, 7135.
- 102 G. Cheng, D. Romero, G. T. Fraser and A. R. Hight Walker, *Langmuir*, 2005, **21**, 12055.
- 103 M. P. Pileni, *Phys. Chem. Chem. Phys.*, 2010, **12**, 11821.
- 104 J. Zeng, J. Huang, W. Lu, X. Wang, B. Wang, S. Zhang and J. Hou, *Adv. Mater.*, 2007, **19**, 2172.
- 105 Y. Lee, H. Lee, P. B. Messersmith and T. G. Park, *Macromol. Rapid Commun.*, 2010, **31**, 2109.
- 106 S. B. Darling, N. A. Yufa, A. L. Cisse, S. D. Bader and S. J. Sibener, *Adv. Mater.*, 2005, **17**, 2446.
- 107 T. Ogawa, Y. Takahashi, H. Yang, K. Kimura, M. Sakurai and M. Takahashi, *Nanotechnology*, 2006, **17**, 5539.
- 108 Y. J. Oh, C. A. Ross, Y. S. Jung, Y. Wang and C. V. Thompson, *Small*, 2009, **5**, 860.
- 109 C. Jiang and V. V. Tsukruk, *Adv. Mater.*, 2006, **18**, 829.
- 110 G. Aliev, M. A. Correa-Duarte, A. Mamedov, J. W. Ostrander, M. Giersig, L. M. Liz-Marzán and N. A. Kotov, *Adv. Mater.*, 1999, **11**, 1006.
- 111 F. Hua, T. Cui and Y. M. Lvov, *Nano Lett.*, 2004, **4**, 823.
- 112 S. Dey, K. Mohanta and A. J. Pal, *Langmuir*, 2010, **26**, 9627.
- 113 S. P. Li, D. Peyrade, M. Natali, A. Lebib, Y. Chen, U. Ebels, L. D. Buda and K. Ounadjela, *Phys. Rev. Lett.*, 2001, **86**, 1102.
- 114 J. Rothman, M. Klaui, L. Lopez-Diaz, C. A. F. Vaz, A. Bleloch, J. A. C. Bland, Z. Cui and R. Speaks, *Phys. Rev. Lett.*, 2001, **86**, 1098.
- 115 C. J. Jia, L. D. Sun, F. Luo, X. D. Han, L. J. Heyderman, Z. G. Yan, C. H. Yan, K. Zheng, Z. Zhang, M. Takano, N. Hayashi, M. Eltschka, M. Klaui, U. Rudiger, T. Kasama, L. Cervera-Gontard, R. E. Dunin-Borkowski, G. Tzvetkov and J. Raabe, *J. Am. Chem. Soc.*, 2008, **130**, 16968.
- 116 H. Wang, Q.-W. Chen, Y.-B. Sun, M.-S. Wang, L.-X. Sun and W.-S. Yan, *Langmuir*, 2010, **26**, 5957.
- 117 Y. Xiong, J. Ye, X. Y. Gu and Q. W. Chen, *J. Phys. Chem. C*, 2007, **111**, 6998.
- 118 M. Klokkenburg, C. Vonk, E. M. Claesson, J. D. Meeldijk, B. H. Erne and A. P. Philipse, *J. Am. Chem. Soc.*, 2004, **126**, 16706.
- 119 P. Y. Keng, I. Shim, B. D. Korth, J. F. Douglas and J. Pyun, *ACS Nano*, 2007, **1**, 279.
- 120 M. J. Hu, Y. Lu, S. Zhang, S. R. Guo, B. Lin, M. Zhang and S. H. Yu, *J. Am. Chem. Soc.*, 2008, **130**, 11606.
- 121 Y. Chu, J. Hu, W. Yang, C. Wang and J. Z. Zhang, *J. Phys. Chem. B*, 2006, **110**, 3135.
- 122 F. Zhang and C.-C. Wang, *J. Phys. Chem. C*, 2008, **112**, 15151.
- 123 T. Ozdemir, D. Sandal, M. Culha, A. Sanyal, N. Z. Atay and S. Bucak, *Nanotechnology*, 2010, **21**, 125603.
- 124 W. Zhang, J. Sun, T. Bai, C. Wang, K. Zhuang, Y. Zhang and N. Gu, *ChemPhysChem*, 2010, **11**, 1867.
- 125 Y. Bao, M. Beerman and K. M. Krishnan, *J. Magn. Magn. Mater.*, 2003, **266**, L245.
- 126 T. C. Lubensky, *Solid State Commun.*, 1997, **102**, 187.
- 127 I. Lisiecki, P. A. Albouy and M. P. Pileni, *Adv. Mater.*, 2003, **15**, 712.

- 128 I. Lisiecki, P. A. Albouy and M. P. Pileni, *J. Phys. Chem. B*, 2004, **108**, 20050.
- 129 I. Lisiecki, D. Parker, C. Salzemann and M. P. Pileni, *Chem. Mater.*, 2007, **19**, 4030.
- 130 O. Kasyutich, R. D. Desautels, B. W. Southern and J. van Lierop, *Phys. Rev. Lett.*, 2010, **104**, 127205.
- 131 M. Sachan, N. D. Walrath, S. A. Majetich, K. Krycka and C.-C. Kao, *J. Appl. Phys.*, 2006, **99**, 08C302.
- 132 F. Luis, F. Petroff, J. M. Torres, L. M. García, J. Bartolomé, J. Carrey and A. Vaurès, *Phys. Rev. Lett.*, 2002, **88**, 217205.
- 133 J. L. Dormann, D. Fiorani and E. Tronc, *Adv. Chem. Phys.*, 1997, **98**, 283.
- 134 P. Jonsson, M. F. Hansen, P. Svedlindh and P. Nordblad, *J. Magn. Magn. Mater.*, 2001, **226**, 1315.
- 135 D. Parker, F. Ladieu, E. Vincent, G. Méridet, E. Dubois, V. Dupuis and R. Perzynski, *J. Appl. Phys.*, 2005, **97**, 10A502.
- 136 J. P. Liu, E. Fullerton, O. Gutfleisch and D. J. Sellmyer, *Nanoscale Magnetic Materials and Applications*, Springer, Berlin, 2009.
- 137 N. Hadacek, A. Nosov, L. Ranno, P. Strobel and R.-M. Galera, *J. Phys.: Condens. Matter*, 2007, **19**, 48620.
- 138 A. Ney, T. Kammermeier, V. Ney, K. Ollefs and S. Ye, *J. Magn. Magn. Mater.*, 2008, **320**, 3341.
- 139 S. Foner, *Rev. Sci. Instrum.*, 1959, **30**, 548.
- 140 *IFF Ferienkurs Magnetismus von Festkörpern und Grenzflächen*, ed. P. Bruno, P. H. Dederichs, P. Grünberg and W. Zinn, 1993, vol. 24, p. 24.1.
- 141 B. D. Josephson, *Rev. Mod. Phys.*, 1974, **46**, 251.
- 142 C. Binek, S. Polisetty, X. He, T. Mukherjee, R. Rajesh and J. Redepenning, *Phys. Rev. B: Condens. Matter Mater. Phys.*, 2006, **74**, 054432.
- 143 <http://www.qdusa.com/sitedocs/productBrochures/1014-003.pdf>.
- 144 M. Hatridge, R. Vijay, D. H. Slichter, J. Clarke and I. Siddiqi, *Phys. Rev. B: Condens. Matter Mater. Phys.*, 2011, **83**, 134501.
- 145 V. F. Puentes, K. Krishnan and A. P. Alivisatos, *Top. Catal.*, 2002, **19**, 145.
- 146 Z. L. Wang, Z. Dai and S. Sun, *Adv. Mater.*, 2000, **12**, 1944.
- 147 W. Kleemann, O. Petravic, C. Binek, G. N. Kakazei, Y. G. Pogorelov, J. B. Sousa, S. Cardoso and P. P. Freitas, *Phys. Rev. B: Condens. Matter*, 2001, **63**, 134423.
- 148 X. Chen, O. Sichelshmidt, W. Kleemann, O. Petravic, C. Binek, J. B. Sousa, S. S. Cardoso and P. P. Freitas, *Phys. Rev. Lett.*, 2002, **89**, 137203.
- 149 O. Petravic, S. Sahoo, C. Binek, W. Kleemann, J. B. Sousa, S. Cardoso and P. P. Freitas, *Phase Transform.*, 2003, **76**, 367.
- 150 S. Bedanta and W. Kleemann, *J. Phys. D: Appl. Phys.*, 2009, **42**, 013001.
- 151 S. Bedanta, O. Petravic, X. Chen, J. Rhensius, S. Bedanta, E. Kentzinger, U. Ruecker, T. Brueckel, A. Doran, A. Scholl, S. Cardoso, P. P. Freitas and W. Kleemann, *J. Phys. D: Appl. Phys.*, 2010, **43**, 474002.
- 152 O. Petravic, *Superlattices Microstruct.*, 2010, **47**, 569.
- 153 M. A. Ruderman and C. Kittel, *Phys. Rev.*, 1954, **96**, 99.
- 154 T. Kasuya, *Prog. Theor. Phys.*, 1956, **16**, 45.
- 155 K. Yosida, *Phys. Rev.*, 1957, **106**, 893.
- 156 K. G. Wilson, *Phys. Rev. B: Solid State*, 1971, **4**, 3174.
- 157 L. P. Kadanoff, W. Götz, D. Hamblen, R. Hecht, E. A. S. Lewis, V. V. Palciauskas, M. Rayl and J. Swift, *Rev. Mod. Phys.*, 1967, **39**, 395.
- 158 C. Domb and M. S. Green, *Phase Transitions and Critical Phenomena*, Academic Press, New York, 1972.
- 159 N. D. Mermin and H. Wagner, *Phys. Rev. Lett.*, 1966, **17**, 1133.
- 160 L. Onsager, *Phys. Rev.*, 1944, **65**, 117.
- 161 D. S. Schmool, R. Rocha, J. B. Sousa, J. A. M. Santos, G. N. Kakazei, J. S. Garitaonandia and L. Lezama, *J. Appl. Phys.*, 2007, **101**, 103907.
- 162 M. Evangelisti, A. Candini, A. Ghirri, M. Affronte, G. W. Powell, I. A. Gass, P. A. Wood, S. Parsons, E. K. Brechin, D. Collison and S. L. Heath, *Phys. Rev. Lett.*, 2006, **97**, 167202.
- 163 W. H. Meiklejohn and C. P. Bean, *Phys. Rev.*, 1956, **105**, 904.
- 164 W. H. Meiklejohn and C. P. Bean, *Phys. Rev. Lett.*, 1957, **102**, 1413.
- 165 J. Nogués, *Internet J. Nanotechnol.*, 2005, **2**, 23.
- 166 C. Binek, *Phys. Rev. B: Condens. Matter Mater. Phys.*, 2004, **70**, 014421.
- 167 C. Binek, X. He and S. Polisetty, *Phys. Rev. B: Condens. Matter Mater. Phys.*, 2005, **72**, 054408.
- 168 S. Polisetty, S. Sahoo and C. Binek, *Phys. Rev. B: Condens. Matter Mater. Phys.*, 2007, **76**, 184423.
- 169 G. Binnig and H. Rohrer, *Helv. Phys. Acta*, 1982, **55**, 726.
- 170 G. Binnig, H. Rohrer, C. Gerber and E. Weibel, *Phys. Rev. Lett.*, 1982, **49**, 57.
- 171 C. Gerber and H. P. Lang, *Nat. Nanotechnol.*, 2006, **1**, 3.
- 172 G. Binnig and H. Rohrer, *Rev. Mod. Phys.*, 1987, **59**, 615.
- 173 S. N. Magonov and M.-H. Whangbo, *Surface Analysis with STM and AFM: Experimental and Theoretical Aspects of Image Analysis*, VCH, New York, 1996.
- 174 U. Hartmann, *Annu. Rev. Mater. Sci.*, 1999, **29**, 53.
- 175 M. E. McConney, S. Singamaneni and V. V. Tsukruk, *Polym. Rev.*, 2010, **50**, 235.
- 176 S. Porthun, L. Abelmann and C. Lodder, *J. Magn. Magn. Mater.*, 1998, **182**, 238.
- 177 L. Folks and R. C. Woodward, *J. Magn. Magn. Mater.*, 1998, **190**, 28.
- 178 M. Kleiber, F. Kümmerlen, M. Löhndorf, A. Wadas and R. Wiesendanger, *Phys. Rev. B: Condens. Matter*, 1998, **58**, 5563.
- 179 S. Gider, J. Shi, D. D. Awschalom, P. F. Hopkins, K. F. Campman, A. C. Gossard, A. D. Kent and S. von Molnar, *Appl. Phys. Lett.*, 1996, **69**, 3269.
- 180 D. H. Qin, H. Yi, H. L. Li, L. Cao and J. B. Ding, *Chem. Phys. Lett.*, 2001, **350**, 51.
- 181 Y. G. Guo, L. J. Wan, C. F. Zhu, D. L. Yang, D. M. Chen and C. L. Bai, *Chem. Mater.*, 2003, **15**, 664.
- 182 C. S. Neves, P. Quaresma, P. V. Baptista, P. A. Carvalho, J. P. Araújo, E. Pereira and P. Eaton, *Nanotechnology*, 2010, **21**, 305706.
- 183 V. F. Puentes, P. Gorostiza, D. M. Aruguete, N. G. Bastus and A. P. Alivisatos, *Nat. Mater.*, 2004, **3**, 263.
- 184 S. Sun, S. Anders, H. F. Hamann, J.-U. Thiele, J. E. E. Baglin, T. Thomson, E. E. Fullerton, C. B. Murray and B. D. Terris, *J. Am. Chem. Soc.*, 2002, **124**, 2884.
- 185 G. E. Moore, *Electronics*, 1965, **38**, 114.
- 186 S. N. Piramanayagam, *J. Appl. Phys.*, 2007, **102**, 011301.
- 187 D. Weller and A. Moser, *IEEE Trans. Magn.*, 1999, **35**, 4423.
- 188 M. E. Schabes, E. E. Fullerton and D. T. Margulies, *IEEE Trans. Magn.*, 2001, **37**, 1432.
- 189 J. Honolka, T. Y. Lee, K. Kuhnke, A. Enders, R. Skomski, S. Bornemann, S. Mankovsky, J. Minár, J. Staunton, H. Ebert, M. Hessler, K. Fauth, G. Schütz, A. Buchsbaum, M. Schmidt, P. Varga and K. Kern, *Phys. Rev. Lett.*, 2009, **102**, 067207.
- 190 H. Katayama, S. Sawamura, Y. Ogimoto, J. Nakajima, K. Kojima and K. Ohta, *J. Magn. Soc. Jpn.*, 1993, **23**, 233.
- 191 H. J. Richter, A. Y. Dobin, O. Heinonen, K. Z. Gao, R. J. M. v. d. Veerdonk, R. T. Lynch, J. Xue, D. Weller, P. Asselin, M. F. Erden and R. M. Brockie, *IEEE Trans. Magn.*, 2006, **42**, 2255.
- 192 A. Kikitsu, Y. Kamata, M. Sakurai and K. Naito, *IEEE Trans. Magn.*, 2007, **43**, 3685.
- 193 D. Sellmyer and R. Skomski, *Advanced Magnetic Nanostructures*, Springer-Verlag, New York, 2006.
- 194 C. Carbone, S. Gardonio, P. Moras, S. Lounis, M. Heide, G. Bihlmayer, N. Atodiresci, P. H. Dederichs, S. Blügel, S. Vlaica, A. Lehnert, S. Ouazi, S. Rusponi, H. Brune, J. Honolka, A. Enders, K. Kern, S. Stepanow, C. Krull, T. Balashov, A. Mugarza and P. Gambardella, *Adv. Funct. Mater.*, 2011, **21**, 1212.
- 195 S. Sun, C. B. Murray, D. Weller, L. Folks and A. Moser, *Science*, 2000, **17**, 1989.
- 196 K. K. Likharev, *Proc. IEEE*, 1999, **7**, 606.
- 197 C. Dupas, P. Houdy and M. Lahmani, *Nanoscience: Nanotechnologies and Nanophysics*, Springer-Verlag, Berlin Heidelberg, 2007.
- 198 A. Nabok, *Organic and Inorganic Nanostructures*, Artech House, 2005.
- 199 M. E. Flatté, *IEEE Trans. Electron Devices*, 2007, **54**, 907.
- 200 S. D. Bader, *Rev. Mod. Phys.*, 2006, **78**, 1.
- 201 S. A. Wolf, D. D. Awschalom, R. A. Buhrman, J. M. Daughton, S. von Molnar, M. L. Roukes, A. Y. Chtchelkanova and D. M. Treger, *Science*, 2001, **294**, 1488.
- 202 M. Tanaka, *J. Cryst. Growth*, 2005, **278**, 25.
- 203 A. Fert, *Thin Solid Films*, 2008, **517**, 2.
- 204 H. Zabel, *Superlattices Microstruct.*, 2009, **46**, 541.

- 205 M. N. Baibich, J. M. Broto, A. Fert, F. Nguyen van Dau, F. Petroff, P. Etienne, G. Creuzet, A. Friederich and J. Chazelas, *Phys. Rev. Lett.*, 1988, **61**, 2472.
- 206 G. Binasch, P. Grunberg, F. Saurenbach and W. Zinn, *Phys. Rev. B*, 1989, **39**, 4828.
- 207 J. S. Moodera, L. R. Kinder, T. M. Wong and R. Meservey, *Phys. Rev. Lett.*, 1995, **74**, 3273.
- 208 S. S. P. Parkin, C. Kaiser, A. Panchula, P. M. Rice, B. Hughes, M. Samant and S.-H. Yang, *Nat. Mater.*, 2004, **3**, 862.
- 209 S. Yuasa, T. Nagahama, A. Fukushima, Y. Suzuki and K. Ando, *Nat. Mater.*, 2004, **3**, 868.
- 210 E. Y. Tsybal, O. N. Mryasov and P. R. LeClair, *J. Phys.: Condens. Matter*, 2003, **15**, R109.
- 211 E. Y. Tsybal, K. D. Belashchenko, J. P. Velev, S. S. Jaswal, M. van Schilfgaarde, I. I. Oleynik and D. A. Stewart, *Prog. Mater. Sci.*, 2007, **52**, 401.
- 212 W. J. Gallagher and S. S. P. Parkin, *IBM J. Res. Dev.*, 2006, **50**, 5.
- 213 D. D. Awschalom and M. E. Flatte, *Nat. Phys.*, 2007, **3**, 153.
- 214 H. Ohno, *Science*, 1998, **281**, 951.
- 215 T. Dietl, *Semicond. Sci. Technol.*, 2002, **17**, 377.
- 216 T. Dietl, H. Ohno, F. Matsukura, J. Cibert and D. Ferrand, *Science*, 2000, **287**, 1019.
- 217 B. T. Jonker, G. Kioseoglou, A. T. Hanbicki, C. H. Li and P. E. Thompson, *Nat. Phys.*, 2007, **3**, 542.
- 218 S. P. Dash, S. Sharma, R. S. Patel, M. P. de Jong and R. Jansen, *Nature*, 2009, **462**, 491.
- 219 C. Binek and B. Doudin, *J. Phys.: Condens. Matter*, 2005, **17**, L39.
- 220 J. P. Velev, P. A. Dowben, E. Y. Tsybal, S. J. Jenkins and A. N. Caruso, *Surf. Sci. Rep.*, 2008, **63**, 400.
- 221 V. Garcia, M. Bibes, L. Bocher, S. Valencia, F. Kronast, A. Crassous, X. Moya, S. Enouz-Vedrenne, A. Gloter, D. Imhoff, C. Deranlot, N. D. Mathur, S. Fusil, K. Bouzehouane and A. Barthélémy, *Science*, 2010, **327**, 1106.
- 222 E. Y. Tsybal and D. G. Pettifor, *Solid State Physics*, ed. H. Ehrenreich and F. Spaepen, Academic Press, 2001, vol. 56, p. 113.
- 223 A. E. Berkowitz, J. R. Mitchell, M. J. Carey, A. P. Young, S. Zhang, F. E. Spada, F. T. Parker, A. Hutten and G. Thomas, *Phys. Rev. Lett.*, 1992, **68**, 3745.
- 224 A. Milner, A. Gerber, B. Groisman, M. Karpovsky and A. Gladkikh, *Phys. Rev. Lett.*, 1996, **76**, 475.
- 225 S. Sankar, A. E. Berkowitz and D. J. Smith, *Phys. Rev. B: Condens. Matter*, 2000, **62**, 14273.
- 226 M. Holdenried and M. Micklitz, *Eur. Phys. J. B*, 2000, **13**, 205.
- 227 J. Inoue and S. Maekawa, *Phys. Rev. B: Condens. Matter*, 1996, **53**, R11927.
- 228 B. J. Hattink, M. García del Muro, Z. Konstantinović, X. Batlle, A. Labarta and M. Varela, *Phys. Rev. B: Condens. Matter Mater. Phys.*, 2006, **73**, 045418.
- 229 J. Barnaš and A. Fert, *Phys. Rev. Lett.*, 1998, **80**, 1058.
- 230 S. Takahashi and S. Maekawa, *Phys. Rev. Lett.*, 1998, **80**, 1758.
- 231 K. Majumdar and S. Hershfield, *Phys. Rev. B: Condens. Matter*, 1998, **57**, 11521.
- 232 A. Brataas, Y. V. Nazarov, J. Inoue and G. E. W. Bauer, *Phys. Rev. B: Condens. Matter*, 1999, **59**, 93.
- 233 S. Mitani, S. Takahashi, K. Takanashi, Y. Yakushiji, S. Maekawa and H. Fujimori, *Phys. Rev. Lett.*, 1998, **81**, 2799.
- 234 T. Zhu and Y. J. Wang, *Phys. Rev. B: Condens. Matter*, 1999, **60**, 11918.
- 235 K. Yakushiji, F. Ernult, H. Imamura, K. Yamane, S. Mitani, K. Takanashi, S. Takahashi, S. Maekawa and H. Fujimori, *Nat. Mater.*, 2005, **4**, 57.
- 236 K. Yakushiji, F. Ernult, S. Mitani, K. Takanashi and H. Fujimori, *Phys. Rep.-Rev. Sec. Phys. Lett.*, 2007, **451**, 1.
- 237 A. Ney, K. Ollefs, S. Ye, T. Kammermeier, V. Ney, T. C. Kaspar, S. A. Chambers, F. Wilhelm and A. Rogalev, *Phys. Rev. Lett.*, 2008, **100**, 157201.
- 238 N. Akdogan, A. Nefedov, K. Westerholt, H. Zabel, H.-W. Becker, C. Somsen, R. Khaibullin and L. Tagirov, *J. Phys. D: Appl. Phys.*, 2008, **41**, 165001.
- 239 S. Hatamie, M. V. Kulkarni, S. D. Kulkarni, R. S. Ningthoujam, R. K. Vasta and S. N. Kale, *J. Magn. Magn. Mater.*, 2010, **322**, 3926.
- 240 N. T. K. Thanh and L. A. W. Green, *Nano Today*, 2010, **5**, 213.
- 241 W. H. Suh, K. S. Suslick, G. D. Stucky and Y. H. Suh, *Prog. Neurobiol.*, 2009, **87**, 133.
- 242 K. E. Kellar, D. K. Fujii, W. H. H. Gunther, K. Briley-Sæbø, A. Bjørnerud, M. Spiller and S. H. Koenig, *J. Magn. Reson. Imaging*, 2000, **11**, 488.
- 243 S. P. Massia, J. Stark and D. S. Letbetter, *Biomaterials*, 2000, **21**, 2253.
- 244 Z. P. Chen, Y. Zhang, S. Zhang, J. G. Xia, J. W. Liu, K. Xu and N. Gu, *Colloids Surf., A*, 2008, **316**, 210.
- 245 J. Xie, C. Xu, N. Kohler, Y. Hou and S. Sun, *Adv. Mater.*, 2007, **19**, 3163.
- 246 J. Xie, C. Xu, Z. Xu, Y. Hou, K. Young, S. Wang, N. Pourmond and S. Sun, *Chem. Mater.*, 2006, **18**, 5401.
- 247 R. De Palma, S. Peeters, M. J. Van Bael, H. Van den Rul, K. Bonroy, W. Laureyn, J. Mullens, G. Borghs and G. Maes, *Chem. Mater.*, 2007, **19**, 1821.
- 248 C. Xu, J. Xie, D. Ho, C. Wang, N. Kohler, E. G. Walsh, J. R. Morgan, Y. E. Chin and S. Sun, *Angew. Chem., Int. Ed.*, 2008, **47**, 173.
- 249 C. Xu, B. Wang and S. Sun, *J. Am. Chem. Soc.*, 2009, **131**, 4216.
- 250 N. Kohler, C. Sun, A. Fichtenholtz, J. Gunn, C. Fang and M. Zhang, *Langmuir*, 2005, **21**, 8858.
- 251 R. Jurgons, C. Seliger, A. Hilpert, L. Trahms and S. Odenbach, *J. Phys.: Condens. Matter*, 2006, **18**, S2893.
- 252 C. Alexiou, R. Jurgons, R. Schmid, A. Hilpert, C. Bergemann, F. Parak and H. Iro, *J. Magn. Magn. Mater.*, 2005, **293**, 389.
- 253 F. X. Hu, K. G. Neoh and E. T. Kang, *Biomaterials*, 2006, **27**, 5725.
- 254 R. Zhang, X. Wang, C. Wu, M. Song, J. Li, G. Lv, J. Zhou, C. Chen, Y. Dai, F. Gao, D. Fu, X. Li, Z. Guan and B. Chen, *Nanotechnology*, 2006, **17**, 3622.
- 255 M. Arruebo, R. Fernandez-Pacheco, S. Irusta, J. Arbiol, M. R. Ibarra and J. Santamaria, *Nanotechnology*, 2006, **17**, 4057.
- 256 R. E. Port, C. Schuster, C. R. Port and P. Bachert, *Cancer Chemother. Pharmacol.*, 2006, **58**, 607.
- 257 H. B. Na, I. C. Song and T. Hyeon, *Adv. Mater.*, 2009, **21**, 2133.
- 258 R. Hao, R. Xing, Z. Xu, Y. Hou, S. Gao and S. Sun, *Adv. Mater.*, 2010, **22**, 2729.
- 259 Y. W. Jun, Y. M. Huh, J. S. Choi, J. H. Lee, H. T. Song, S. Kim, S. Yoon, K. S. Kim, J. S. Shin, J. S. Suh and J. Cheon, *J. Am. Chem. Soc.*, 2005, **127**, 5732.
- 260 F. Hu, L. Wei, Z. Zhou, Y. Ran, Z. Li and M. Gao, *Adv. Mater.*, 2006, **18**, 2553.
- 261 C. Sun, O. Veiseh, J. Gunn, C. Fang, S. Hansen, D. Lee, R. Sze, R. G. Ellenbogen, J. Olson and M. Zhang, *Small*, 2008, **4**, 372.
- 262 J. H. Lee, Y. M. Huh, Y. W. Jun, J. W. Seo, J. T. Jang, H. T. Song, S. Kim, E. J. Cho, H. G. Yoon, J. S. Suh and J. Cheon, *Nat. Med.*, 2007, **13**, 95.
- 263 D. Shi, *Adv. Funct. Mater.*, 2009, **19**, 3356.
- 264 H. Yu, M. Chen, P. M. Rice, S. X. Wang, R. L. White and S. H. Sun, *Nano Lett.*, 2005, **5**, 379.
- 265 J. Gao, H. Gu and B. Xu, *Acc. Chem. Res.*, 2009, **42**, 1097.
- 266 R. Hergt, S. Dutz, R. Muller and M. Zeisberger, *J. Phys.: Condens. Matter*, 2006, **18**, S2919.
- 267 R. Hergt, W. Andra, C. G. d'Ambly, I. Hilger, W. A. Kaiser, U. Richter and H. G. Schmidt, *IEEE Trans. Magn.*, 1998, **34**, 3745.
- 268 A. Jordan, R. Scholz, P. Wust, H. Fling and F. Roland, *J. Magn. Magn. Mater.*, 1999, **201**, 413.
- 269 P. Wust, B. Hildebrandt, G. Sreenivasa, B. Rau, J. Gellermann, H. Riess, R. Felix and P. M. Schlag, *Lancet Oncol.*, 2002, **3**, 487.
- 270 L. M. Lacroix, D. Ho and S. H. Sun, *Curr. Top. Med. Chem.*, 2010, **10**, 1184.
- 271 M. Rycenga, C. M. Cobley, J. Zeng, W. Li, C. Moran, Q. Zhang, D. Qin and Y. Xia, *Chem. Rev.*, 2011, **111**, 3669.
- 272 H. Ko, S. Singamaneni and V. V. Tsukruk, *Small*, 2008, **4**, 1576.